International Journal of Disaster Risk Reduction 108 (2024) 104508

Contents lists available at ScienceDirect

International Journal of Disaster Risk Reduction

journal homepage: www.elsevier.com/locate/ijdrr

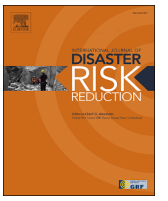

A framework for multi-risk assessment in a historical area of Lisbon

G. Mascheri [a, *], N. Chieffo [a], C. Arrighi [b], C. Del Gaudio [c], P.B. Lourenço [a]

[a] University of Minho, ISISE, ARISE, Department of Civil Engineering, Guimarães, Portugal
[b] Department of Civil and Environmental Engineering, University of Florence, Via di S. Marta 3, 50139, Florence, Italy
[c] Department of Structures for Engineering and Architecture, University of Naples Federico II, Via Claudio 21, 80125, Naples, Italy

ARTICLE INFO

Keywords:
Multi-hazard
Multi-vulnerability assessment
Seismic vulnerability
Flood vulnerability
Multi-risk assessment
Loss estimation

ABSTRACT

Historic areas have faced escalating risks due to population growth, urbanization, climate change, and increasing public awareness. Existing risk assessment methods often focus on individual hazards, necessitating a more integrated approach. This research introduces a comprehensive multi-risk model to assess the potential impacts of rainfall and earthquakes on Lisbon's historic city centre. The model considers key risk components – hazard, exposure, and vulnerability – providing a detailed evaluation. Pluvial flood hazards for different return periods were analysed using a proper hydrological model, and seismic hazards were estimated based on PGA values (0.035g–0.25g) with a 10 % exceedance probability over 50 years. Concerning the exposure, the paper integrates spatial distribution data acquired through satellite remote sensing and GIS tools, along with census data. Vulnerability assessments for ordinary unreinforced masonry buildings (URM) used the Risk-UE method and flood stage-damage curves. The results obtained through a multi-exposure and multi-vulnerability framework provide insight into the expected building losses: for a 475/500-year return period, the estimated losses are approximately 1150 M€ for earthquakes and 22 M€ for floods. The higher losses for earthquakes are attributed to structural damage, whereas flood losses are predominantly associated with indirect impacts and loss of contents. This study marks a novelty in the application of risk assessment methodologies in Portugal addressing multiple hazards and highlights the protection of the built environment to mitigate economic and human losses. The paper serves as a starting point for further assessments, offering an overview of the influence of multiple risks on urban settings.

1. Introduction

1.1. Definition of the problem

Natural hazards are expected to become increasingly harmful to communities and urban areas as the severity, frequency but also spatial distribution of catastrophic occurrences have changed [1]. As a result, the topic of assets exposed to hazards has gained significance in recent years, raising community awareness about the issue. Population growth, coastal city expansion, uncontrolled urban development, inadequate multi-level governance, and climate change are among the primary drivers of the rise in exposure to risks [2–5]. The world's average temperature has grown dramatically as a result of the increase in greenhouse gas emissions caused by human activity. By 2100, it is expected that the Earth's temperature will increase from 1 to 5 °C, with higher recurrence of extreme events such as droughts, landslides, floods, heat waves, and fires [3,6]. Indeed, climate and environmental changes have been docu-

* Corresponding author.
E-mail addresses: glenda.mascheri@civil.uminho.pt (G. Mascheri), nicola.chieffo@civil.uminho.pt (N. Chieffo), chiara.arrighi@unifi.it (C. Arrighi), carlo.delgaudio@unina.it (C. Del Gaudio), pbl@civil.uminho.pt (P.B. Lourenço).

https://doi.org/10.1016/j.ijdrr.2024.104508
Received 9 January 2024; Received in revised form 26 March 2024; Accepted 23 April 2024
Available online 27 April 2024

mented for several decades, resulting in a significant influence on natural hazards, with severe repercussions for populations [2,6]. According to Ref. [7] approximately 19 % of the planet's land area and more than half of its inhabitants are severely exposed to at least one hazard. Natural disasters affected more than 1.5 billion people between 2005 and 2015 [8]: more than 700.000 people died, 1.4 million were injured, and around 23 million lost their homes, plus additional individuals who were affected in different ways by these disasters. In terms of monetary losses, it has been estimated that the real cost per year to the global economy due to disasters is around US$ 520 billion [9].

The statistics presented show how the increasing frequency and intensity of severe events have made communities more vulnerable and exposed to hazards, particularly in urban areas, which concentrate a high percentage of the population, infrastructures, and assets in general, putting them at the top of the list of intervention priorities [3–5]. Furthermore, UNESCO World Heritage Sites are equally subject to geological hazards, which can become disasters if the local governments are inadequately prepared [10]. Many studies have been conducted to estimate World Heritage asset's exposure to hazards. For example, a study [11] reported that in Italy, geological hazards affect approximately 70 % of the UNESCO sites. Furthermore, in the analysis of different datasets developed by Ref. [10], noteworthy findings have emerged: almost 60 % of World Heritage Sites are vulnerable to at least one hazard among tsunamis, landslides, earthquakes, and volcanic eruptions. Therefore, the increasing exposure of assets to natural hazards necessitates a procedure for adapting cultural heritage to climate change, i.e. modifying how a system responds to threats. However, the limited research in this field indicates a forthcoming challenge that needs to be addressed [6].

Given the increasing importance of the topic, an international effort has been made: the Hyogo Framework for Action, HFA [12], and the subsequent update UN Sendai Framework for Disaster Risk Reduction 2015–2030 [8], emphasised the need for understanding, assessing and managing risks in exposed urban areas. This issue is particularly problematic for the historical city centres, as their value to communities as prominent testimony of culture and history, as well as their importance as a source of attractiveness and economic development, require special attention [5]. In light of these considerations, the assessment of hazard, vulnerability and risk is important to preserve the built environment, increase the preparedness population, propose more effective disaster reduction plans and reduce economic and human losses [1,4,5].

1.2. Risk terminology

The terminology related to risk can be found with different connotations within the scientific literature [4], therefore a brief explanation of the main terms is useful. The term risk is usually defined as "*the combination of the probability of an event and its negative consequences*" [13] and can be intended as a combination of three terms, hazard, vulnerability and exposure [14], resulting in the well-known risk equation:

$$R = H \cdot V \cdot E \tag{1}$$

where R is the risk, H is the hazard, V is the vulnerability and E is the exposure. The hazard term is defined as "*a process, phenomenon or human activity that may cause loss of life, injury or other health impacts, property damage, social and economic disruption or environmental degradation*" [15], i.e. a physical phenomenon (e.g. earthquake, flood or sea level rise) with the capacity to inflict damage and loss to different assets [1]. Vulnerability can be defined as "*the conditions determined by physical, social, economic and environmental factors or processes which increase the susceptibility of an individual, a community, assets or systems to the impacts of hazards*" [15], i.e. the predisposition of an asset to be negatively impacted by a certain hazard [1]. The definition of exposure is "*the situation of people, infrastructure, housing, production capacities and other tangible human assets located in hazard-prone areas*" [15], i.e. the presence of assets in potentially hazardous areas [1].

In light of [16], it is important to point out that in the 1970s and early 1980s, the vulnerability concept was primarily related to physical fragility, and can be defined as the degree of loss of a specific element at risk caused by a specific hazard, represented as a percentage of loss ranging from 0 (no damage) to 1 (total damage), as explained in Ref. [17]. However, the concept of vulnerability evolved, including not only the physical fragility but also the socio-cultural, economic, environmental, and political dimensions, as well as the capacity to cope and recover from the negative effects of a disaster event [16,17]. As a result [16], stated that a dual notion of vulnerability that combines susceptibility and coping capacities, and that encompasses different dimensions, led to a variety of slightly different vulnerability connotations and approaches, see Refs. [17–20]. In this context, the risk term evolved alongside the other concepts, thus [15] defines a "disaster risk" as "*the potential loss of life, injury, or destroyed or damaged assets which could occur to a system, society or a community in a specific period, determined probabilistically as a function of hazard, exposure, vulnerability and capacity*". The term "capacity" refers to both being able to cope, which refers to short-term reactions to events, and adaptive capacity, which refers to long-term risk-reduction measures. Due to this, the adaptive capacity may modify an asset vulnerability, by improving the capacity to cope, as well as the asset exposure [4,20]. This new notion is consistent with the understanding, which gained prominence in the 1990s, that disaster adaptation is inevitable since climate change is already occurring and the consequences are unavoidable [6]. Therefore, a new risk concept can be defined as [21]:

$$\text{Risk} = \frac{\text{Hazard} \cdot \text{Exposure} \cdot \text{Vulnerability}}{\text{Capacity}} \tag{2}$$

The evolution of the aforementioned concepts has inspired the development of different risk assessment methods, leading to a more comprehensive and interdisciplinary vision [22]. Moreover, in recent years, a further evolution of hazard, vulnerability and risk assessment has moved towards a multi-hazard perspective, since many places throughout the world are vulnerable to a range of hazards, and an effective response plan should take these multiple threats into account [5,21].

1.3. Multi-hazard context

As mentioned above, risk mitigation has gained importance and, consequently, several methods for determining hazard, vulnerability and risk have been developed. The temporal or spatial overlap of multiple hazards in a given location results in a multi-hazard context [4,23]. Despite this, fewer approaches have been dedicated to investigating multiple hazards concurrently, instead analysing one hazard at a time, especially for historical city centres [24–26]. According to Ref. [4] a multi-hazard approach for risk assessment and disaster management was first stated in Agenda 21 [27] to define strategies for sustainable urban development. This requirement was reaffirmed in the Johannesburg Declaration of Sustainable Development in 2002 [28] and later, the Hyogo Framework of Action [12] and the UN Sendai, emphasised the need for a multi-hazard approach [8]. The UN Sendai statement expressly mentions the idea that risk reduction practises must be as "*multi-hazard and multisectoral*" as feasible, and risks must be mitigated by a deep understanding of hazard, vulnerability, capacity and exposure to multiple hazards. The "*multi-hazard approach*" is the base of an efficient disaster risk reduction strategy, as stated in the guideline principles of [8].

The problem of disaster risk reduction (DRR) is essential not only for preventing losses and safeguarding ecosystems and human lives but also for the preservation of historical city centres. Indeed, historic centres are particularly vulnerable because they have a dual value: their physical or tangible value which results in economic relevance, and their immaterial value which includes social value, historical value and associated traditions, community identity and memory, as well as the sense of belonging [6,24]. Despite the international effort to reduce disaster risk, multi-hazard assessment approaches are still not well established. Indeed, the technical understanding, the expertise, as well as the significant financial investment required, make this topic difficult to develop. An additional challenge is how to assess vulnerability and losses that may arise, due to different metric systems and process characteristics for each hazard. These issues become particularly acute in historic city centres, where the complex nature of the physical environment highlights the challenges of multi-risk assessment with the aim of conservation [5,24,26]. Multi-hazard impacts are more than the sum of the individual hazards examined and the total level of risk may be affected by hazard interrelations that result from their spatial and temporal overlap [23,26]. As a result, adopting a standardised approach that takes into account the numerous possibilities of hazard combinations remains complex [26]. In this regard, a definition of a common multi-hazard language might be beneficial in building a consistent strategy. Consequently, several authors [1,21,23,29] have made an effort to clarify the terminology related to multiple hazards. Starting from a general point of view [29] distinguish the terms "*multi-layer single-hazard*" and "*multi-hazard*". The first one refers to a general strategy that can involve both the identification of areas where many hazards overlap and the independent analysis of various hazards within a given area. Contrarily, the term "*multi-hazard*" should also consider the relationships between the various hazards. Ref. [1] describes multi-hazard language depending on the risk component (hazard, vulnerability, or risk). When two or more hazards overlap geographically with or without temporal coincidence, the term "*multi-hazard*" is used. Instead, "*multi-vulnerability*" refers to the dynamic aspect of vulnerability: an asset may show different levels of vulnerability to different hazards, but the vulnerability can also change over time. Starting with these two definitions, the term risk may lead to two categories of approaches: "*multi-risk*" and "*multi-hazard risk*". Multi-risk is when the risks are separately assessed with their exposure and vulnerability, and these assessments are then combined into a holistic evaluation that considers all potential hazard and vulnerability relationships. A multi-hazard risk assessment, on the other hand, occurs when a multi-hazard index and a single global vulnerability index are simply combined, resulting in a multi-hazard risk assessment [1].

The definitions of these terms are slightly different from one author to another, however in the present paper "multi-hazard" is used for a general context in which multiple hazards and their interrelations are considered; "multi-vulnerability" is used for different degrees of vulnerability depending on the type of hazard, and "multi-risk" is used for the calculation of the impact, which includes the concepts of multi-hazard and multi-vulnerability. Hazard interactions are undoubtedly an important issue in the multi-hazard context since different types of interactions may result in distinct outcomes as well as different methods for risk mitigation. It is important to note that multiple hazards may have distinct distributions since they can overlap geographically, only temporally, or both spatially and temporally [4]. Different definitions of interactions may be found in the literature [23,29,30], however, according to Ref. [23] they can be divided into five main categories:

- Independence: geographical and temporal overlap of the effects of two or more hazards with no interrelations;
- Triggering or cascading: a primary event causes one or more secondary hazards to occur, resulting in a hazard cascade;
- Change conditions: one hazard might affect how another hazard impacts by altering environmental conditions;
- Compound hazard: different hazards all come from the same "primary event" on a large-scale process, there is no primary or secondary hazard since they happen at the same time;
- Mutual exclusion: it is when two natural hazards are mutually exclusive or may have a negative dependency.

As a consequence of the above, risk assessment for multiple hazards is a complex subject which needs to consider the spatial, temporal and type of hazard interactions, the dynamic nature of exposure and vulnerability, as well as coping capacity. It must be also kept in mind that future decisions in the field of disaster risk reduction have to consider the modifications in the environment due to climate change [1,4]. Due to the complexity of the problem, various literature reviews on multi-hazard approaches have been conducted, trying to establish a generic framework for the multi-hazard context [1,5,23,25,26]. Methodologies can be described using a different classification, for example, the study proposed by Ref. [25] divides them into qualitative, semi-quantitative and quantitative. Qualitative analyses provide qualitative results usually with descriptions in words (e.g. low, medium, high), as depicted in Refs. [4,31–33]. Semi-quantitative methods differ from qualitative ones since they introduce a scale, usually in numbers, which allows to assign relative ranks between hazards [34–37]. Quantitative methods usually address a complete quantitative definition of the problem, allowing for an absolute value on a predefined scale, as reported by Refs. [38,39]. However [26], subdivided different methods

into multi-hazard analysis, vulnerability for multiple hazards analysis, and multi-hazard risk analyses. In the multi-hazard analysis, the intensity of each hazard is evaluated, allowing for the assessment and development of maps concerning the potential occurrence of multiple hazards in a specific location [40–42]. In the analysis of vulnerability to multiple hazards, the assessment considers the dynamic nature of vulnerability. This means that the occurrence of one hazard can influence the vulnerability conditions for another hazard, and the cumulative impact of multiple hazards can modify the overall vulnerability level. Moreover, the same building characteristics may contribute differently to vulnerability depending on the specific hazard under consideration, see Refs. [43–47]. The multi-hazard risk analysis allows for risk evaluation and can be viewed as a combination of the previous two components [14,24,48].

In light of these considerations, the objective of the present study is to provide a thorough multi-risk assessment model that is specifically tailored to historical centres. This study focuses on a multi-risk assessment method that considers the likelihood of earthquakes and pluvial floods, which have already occurred in the city of Lisbon [49,50]. The study evaluates the risk and vulnerability of typical unreinforced masonry structures (URM) in Baixa Pombalina, an important historical area of the city. To begin, the exposure model was developed using remote sensing techniques and then processed into the GIS environment. Then, scenarios for different return periods were simulated, and seismic and flood vulnerability were appropriately assessed using the Risk-UE approach and flood state-damage curves, respectively. Lastly, a multi-risk assessment was performed, which included an assessment of building economic losses to determine financial consequences. The paper is organized as follows: in Section 2 an explication of the materials and methods that have been applied is provided; Section 3 explains the result and discussion of the methodology used in the case study area; in Section 4 further developments of the work are addressed; finally, in Section 5 the main outcomes are discussed.

2. Materials and methods

The multi-risk approach presented assesses risk by combining flood and earthquake threats (multi-hazard) and calculating different vulnerabilities to these distinct hazards (multi-vulnerability). The effort will focus on an urban scale in a historic city centre, using a GIS tool to develop an exposure model to evaluate building losses. It is assumed that the two analysed hazards occur within a short time from one another, with no interactions (independent). Therefore, this multi-risk assessment relates more to a multi-layer single-hazard risk assessment, according to the nomenclature specified in Section 1.3. Indeed, this classification is important because the two discrete hazards in this scenario overlap independently, with the total risk evaluated as the likelihood of two hazards occurring in a short time. For both hazards, the basic elements of the risk equation, i.e. hazard, vulnerability, and exposure, have been determined. It is important to note that the comparison of the two threats takes place through the definition of the return period T_R, but the intensity measures are different: for flood hazard, the most important parameters defined were flood depth and inundation extent, whereas for earthquake hazard is the Peak Ground Acceleration (PGA), which is then converted into EMS-98 intensity [24]. Vulnerability has been assessed following a different procedure for earthquakes and floods since the damage metric systems associated with the two hazards are different. However, the result is a common metric system consisting of physical damage ($D_{\%}$), which allows the evaluation of the percentage of losses concerning global exposure. Consequently, the exposure model serves as a common layer for both hazards allowing the losses for all created scenarios to be compared [24]. The present study introduces a novel framework for evaluating seismic and rainfall-induced flood risks, filling the gap from the conventional research emphasis on either seismic risks or flood risks related to alluvial floods [24,48]. In comparison to the study proposed in Ref. [24], this work includes some new ideas, even though the overall workflow is similar. Both assess the multi-risk of seismic and flood threats in a historic city, treating the two events as independent natural occurrences and comparing scenario losses based on cost aggregation. However, the application to the Italian context [24], with its unique hazard and building characteristics, makes the current work novel for multi-risk assessment in Portugal. There are significant differences in the exposure model. In Ref. [24], the monetary exposure, representing repair costs, was calculated as 20 % of the market value. This approach was validated in other Italian contexts where damage data were accessible. Due to a lack of data in this study, the monetary value is assumed to be the market value, and consequently the losses might be understood as a depreciation of market value. It is also worth noting that in the multi-hazard evaluation in Ref. [24] alluvial flood has been analysed, whereas the current work considers the pluvial flood phenomena. Lastly, although the seismic vulnerability has been evaluated with the same methodology, for the flood vulnerability a different stage-damage curve model has been adopted in the two works.

The procedure was divided into six basic phases, which are discussed next. First, the exposure model was methodically developed by gathering a full inventory of the buildings under consideration with a consistent set of building features, then organized and visualised within the QGIS environment [51]. The second step included a flood hazard assessment, defined by water depth and inundation extent, which involved simulating pluvial flood scenarios for different return periods. Flood vulnerability has been subsequently estimated through the use of stage-damage curves, which relate the intensity parameter (flood depth in metres) to the relative physical damage $\left(D_{\%}^{FL}\right)$. In the fourth step, an earthquake scenario is simulated by estimating the intensity parameter (EMS-98) associated with various return periods. The fifth phase involved assessing seismic vulnerability using the Risk-UE approach, which allows for the calculation of physical damage defined as degree of loss $\left(D_{\%}^{EQ}\right)$. Finally, the multi-risk assessment was evaluated by combining the economic losses produced by two independent hazards, which were expressed as market value depreciation if the two hazards occurred. Fig. 1 depicts the flowchart of the current state of the proposed work.

2.1. Exposure model

The first step to carrying out a risk assessment procedure, especially at an urban scale, is the development of an exposure model. Exposure, vulnerability, and capacity to a certain hazard are required to assess the risk associated with a given hazard over an area [15]. People, properties, economic activities, and private and public services are all examples of risk-exposed assets that can be affected directly or indirectly by a catastrophic event in a specific area [17]. When analysing risk, all assets that may be exposed to haz-

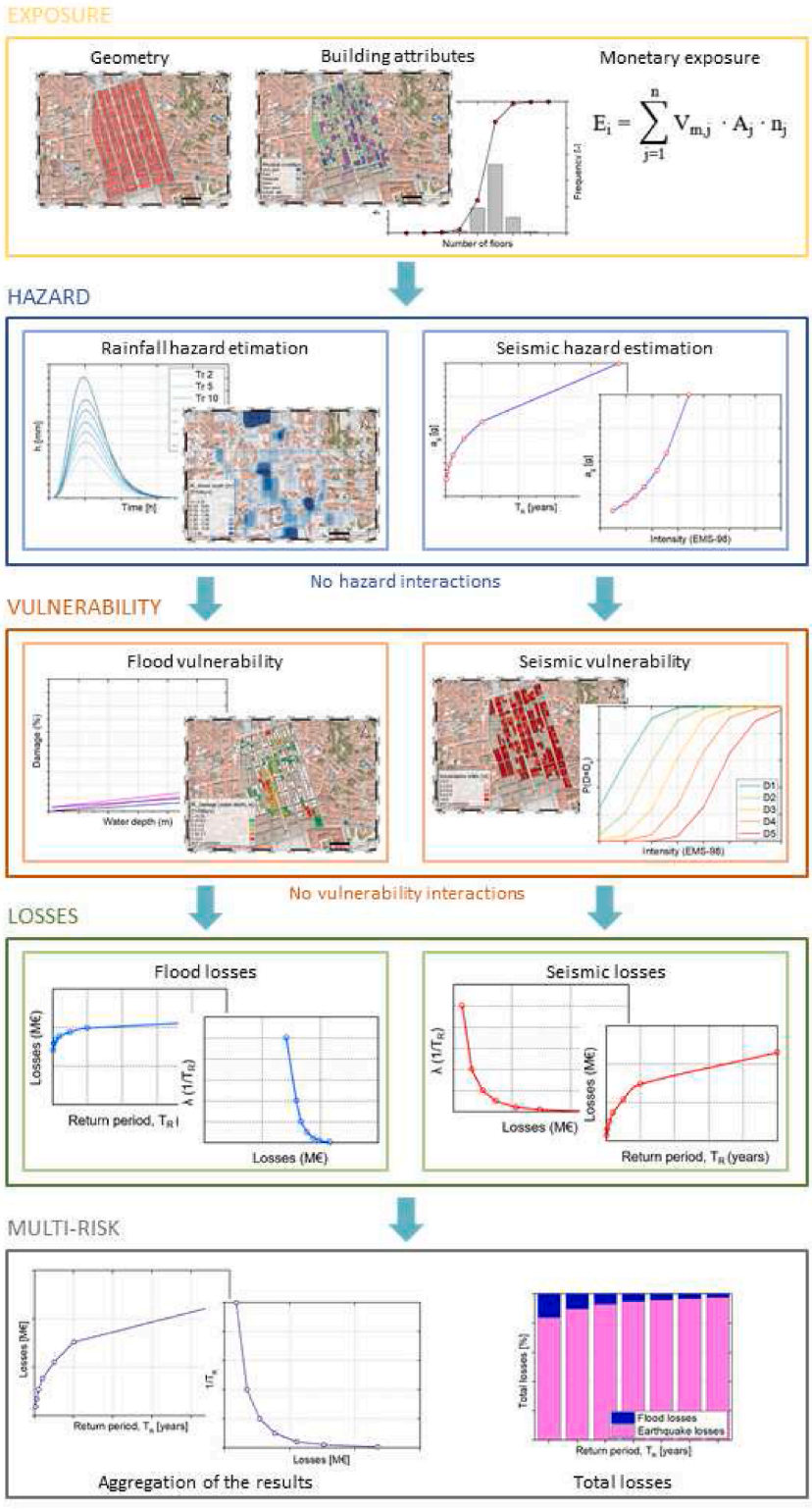

Fig. 1. Flowchart of the applied methodology.

ards should be identified, classified, and organised using an inventory that includes the relevant physical attributes. However, in the current work, the exposure model is restricted to ordinary unreinforced masonry (URM) structures in a subsector of the city of Lisbon. The exposure of a building can be identified by its position and monetary value, and it is an essential spatial data layer to be used for risk assessment, as it allows for the comparison of scenario losses in multi-risk analysis [17,24]. Thus, the exposure model used in the current study, which includes data collection, spatial representation, and monetary exposure, was carefully evaluated.

2.1.1. Collection of data and inventory

Gathering data about the examined buildings and establishing a complete inventory comprising a consistent range of building variables (e.g. building typology, number of storeys, physical condition, position in the aggregate, building function on the ground floor and the existence of a basement) is the first stage for a congruent development of an exposure model. Following that, the spatial representation and storage of the main features can be performed. For the current study, the open-source QGIS software was used for the data gathering and representation [51]. GIS offers a wide range of activities such as graphical representation, data storage, updating, georeferencing, elevation model downloading, and a variety of other analytical processing. This is useful for risk assessment, particularly across vast geographical regions with a large amount of data, allowing for mapping and analysing vulnerability and losses, as well as designing emergency response and management strategies [52]. Data collecting is a key aspect, especially when addressing existing buildings, because data accessibility, availability, and reliability are major concerns [52]. During this phase, all relevant information must be obtained from various sources such as literature, online databases, remote sensing, census statistics, surveys or official databases. However, data availability is not always satisfactory, and most of the time professionals must cope with a shortage or lack of data. In this specific case, the key information acquired was on: location and geomorphologic features; building typology characteristics; flood hazard classification; earthquake hazard classification; and monetary value. Data on building typology characteristics, flood and earthquake hazard classification were acquired from previous and ongoing research, while sources for spatial and geomorphological elements included Google Maps, Google Earth, and GIS. Finally, census data were used to have a better understanding of the monetary exposure. Following the data collecting phase, inventory organisation is an essential stage in the risk assessment method. The current study systematically classified multiple factors such as building type, number of storeys, physical conditions, aggregate position, and ground-level building function. All of this information enabled statistical analysis of the building sample as well as geographical visualisation in the QGIS environment through maps.

2.1.2. Monetary exposure

The monetary exposure of the analysed building sample is obtained by multiplying the floor area, by the market value, and the number of floors, according to the:

$$E_i = \sum_{j=1}^{n} V_{m,j} \cdot A_j \cdot n_j \tag{3}$$

where E_i is the monetary value of the i-building, $V_{m,j}$ is the market value expressed in €/m^2, A_j is the building area and n_j is the number of floors. Normally data about the market value can be found in the census statistics or relevant databases.

2.2. Hazard model

Assessing hazards quantitatively entails determining "*the likely frequency of occurrence of different intensities for different areas, as determined from historical data or scientific analysis*" [13]. Defining the occurrence probability and visualising the hazard distribution intensity within the selected urban area are both steps in the process of building seismic and flood scenarios. Because the intensity measures for the two hazards differ, so does the hazard evaluation method. The most frequent intensity measures for describing seismic severity are macroseismic intensity or Peak Ground Acceleration (PGA) [53]. In particular, the EMS-98 scale, which is often used to estimate macroseismic intensity, offers a measure of the severity of ground shaking based on observed damage [54,55]. In the proposed study, the use of EMS-98 is based on its proven effectiveness and broad use in assessing seismic effects. In the case of a flood event, the intensity is normally determined by using the water depth and inundation extent that may be experienced during the flood event at a specific location for a certain return period [24]. Different types of floods can be modelled, such as pluvial floods (considering rainfall events) or alluvial floods (considering river flooding), although the current case study only considers pluvial floods. Moreover, the area under examination is not susceptible to alluvial floods, as discussed in Section 3.

2.2.1. Flood hazard

The initial step in estimating rainfall-induced hazard is to run pluvial flood simulations for different return periods. These scenarios have been simulated using a hydraulic model in HEC-RAS (Hydrologic Engineering Center, River Analysis System) software [56]. The two main categories of input data required by the HEC-RAS 2D model are topographic data and unsteady flow data. Topographic data are related to spatial information such as the Digital Elevation Model (DEM), 2D flow area, land use and the value of Manning's n coefficient. The DEM has been processed through GIS, in particular through the SRTM (Shuttle Radar Topography Mission) downloader plugin which allows to derive terrain geometry with a resolution of 30 m from NASA earth data. The 2D flow area was also specified, which is a polygon that defines the 2D area's boundary created using the Geometric Data editor 2D flow data drawing tool. Also, in the case of unsteady flow, the upstream discharge (i.e. the direction where the flow begins or comes from, or the upper part of the watercourse) and a downstream discharge-stage rating (the direction where the flow moves or flows, or the lower part of the watercourse) were defined properly [56]. Defining land-use data is crucial for determining Manning's n values within the 2D flow area. This data is essential for accurately characterizing the terrain and optimizing the representation of flow dynamics. These parameters,

often referred to as Manning's roughness coefficients, are parameters used in open-channel hydraulics to quantify the resistance to flow within a channel. The land-use data have been downloaded from the Esri Land Cover website [57], from the Environmental Systems Research Institute, which provides an annual 10-m resolution map of the land surface of the Earth. This map has been created for each year from 2017 to 2022, through the application of existing artificial intelligence land classification models to the Sentinel-2 data [57]. The precipitation input data utilised in HEC-RAS is presented in terms of hyetographs, which are curves that correlate the duration of the event and the corresponding rainfall depth (in millimetres). These hyetographs were derived by dividing the flood hydrographs, calculated using the Soil Conservation Service-Curve Number (SCS–CN) method, by the basin area.

Thus, the hydrographs have been calculated using the SCS-CN approach [58], using observed rainfall data for the site under consideration. Indeed, the collected data from previous occurrences is used to create the IDF curves (intensity-duration-frequency), which indicate the relationship between precipitation intensity and duration associated with a return period for a certain udometric meteorological station.

Using a statistical analysis of previous data and the probability distribution function (Gumbel's law), the precipitation intensities associated with the return periods for different intensity durations are computed. This enables the depiction of rainfall intensity I (mm/h) as a function of rainfall duration (h) for each specific return period. Subsequently, to derive the hydrographs, the SCS-CN method was applied, which is a method for calculating "*the volume of direct surface runoff for a given rainfall event*" based on the water balance equation, which results in [59]:

$$Q = \frac{\left(P - I_a\right)^2}{P - I_a + S} = \frac{(P - \lambda \cdot S)^2}{P + (1 - \lambda) \cdot S} \tag{4}$$

where P is the total precipitation (mm), I_a is the initial abstraction (mm), Q is the direct runoff (mm), S is the potential maximum retention (mm), and λ is the initial abstraction coefficient. This formula relies on two fundamental terms: P can be obtained from IDF curve parameters; S is evaluated with the Curve-Number method. Once the IDFs were estimated, the constants *a* and *n* for defining the hydrographs were calculated using a regression model that describes the rainfall density, as [60]:

$$I = a \cdot t(h)^n \tag{5}$$

where *a* and *n* are constants, I (mm/h) is the intensity and *t* is the duration (h).

It is important to point out that the values of the coefficient *a* vary from a minimum of 176.46 for the return period of 2 years to a maximum of 375.21 for the return period of 500 years. Furthermore, the exponent, n, ranges from $-0.529 < n < -0.451$ associated with the same examined return periods.

Next, the parameter S can be calculated as in the following equation [59,61]:

$$CN = \frac{25400}{S + 254} \tag{6}$$

The CN number is a non-dimensional term and depends on soil groups A, B, C, and D (where A denotes soils with higher infiltration rate and D soils with lower infiltration rate), and a complex classification composed of land-use, treatment and hydrologic condition, and antecedent soil moisture conditions. Indeed, the CN number considers soil moisture levels before the event (Antecedent Moisture Conditions, AMC): AMCI (dry), AMCII (normal), and AMCIII (wet), see Ref. [62] for details. Once the hydrographs were estimated, the corresponding hyetographs were used as the boundary condition in HEC-RAS software [56]. This allows for pluvial flood scenario modelling and the estimation of water depths for different return periods.

2.2.2. Seismic hazard

The seismic hazard was defined in terms of EMS-98 macroseismic intensity [63], with a formula that relates Peak Ground Acceleration (PGA) with EMS-98 intensities used. Specifically, the methodology proceeds with the PGA value for the 475-year return period and then, as explained in Ref. [64], computes PGA values for other return periods using:

$$a_{b|PR=t} = a_{b|PR=T} \cdot \left(\frac{t}{T}\right)^{0.37} \tag{7}$$

where $a_b|_{PR=t}$ is the basic acceleration for a return period *t* and $a_b|_{PR=T}$ is the basic acceleration for the return period of 475 years. The relation between PGA and EMS-98 macroseismic intensity conversion reads [64]:

$$\log_{10}\left(a_b\right) = 0.301030 \cdot I - 0.2321 \tag{8}$$

where a_b is the basic acceleration and I is the macroseismic intensity according to the EMS-98 scale [63].

2.3. Vulnerability model

2.3.1. Flood vulnerability

The flood vulnerability model was developed by adopting stage-damage curves which relate the intensity parameter (flood depth in meters) with the relative physical damage $\left(D_{\%}^{FL}\right)$. This approach finds widespread application, as evidenced by Refs. [24,65,66], where the selection of the proposed stage-damage curves is used for evaluating the structural damage in a building exposed to a spe-

cific water depth. Selecting a damaging grade involves developing a defined category using a damage scale. It also serves to reduce subjectivity, as different stakeholders may define damage differently. It also takes into consideration grading sensitivity as a result of the scale's discrete subdivision. Damage scales typically range from DS0 (no damage) to DS5 (collapse), although their thresholds' definition varies according to the desired level of precision [67,68]. There are damage scales available in the literature for many types of floods: Refs, [69,70] established damage levels to buildings exposed to tsunamis; the classification proposed by Ref. [71], later extended in Ref. [67], proposed seven damage states to classify the damage to some components (e.g. roof, windows, foundation etc.) for wind and flood, as depicted in Ref. [72], Refs. [73,74] proposed five damage states for floods. In the present study, based on the water depth obtained, six damage thresholds were defined to gain insight into the predicted implications of the current scenario, (DF_k = 0, 1, 2 …, 5) where the letter *k* represents the expected damage thresholds, namely: DF0 (no damage); DF1 (very low); DF2 (low); DF3 (moderate); DF4 (high); and DF5 (very high). These correspond to a specific water depth, (h), expressed in meters as reported in Table 1.

2.3.2. Seismic vulnerability

The Risk-UE project [75] developed an index-based technique that has been used to study the seismic vulnerability of structures, as depicted in Ref. [76]. The main objective of this project was to promote the creation of an extensive seismic risk assessment method that all of Europe could use [77]. In this method, buildings are classified into typological classes based on the Building Typology Matrix (BTM), and the vulnerability of each building is computed considering:

$$\overline{V_I} = V_I^* + \Delta V_R + \Delta V_m \tag{9}$$

where V_I^* is the most probable value of the vulnerability index V_I of the corresponding building class, ΔV_R is the regional vulnerability factor that considers, on a regional scale, the specific quality of the building types derived from expert opinion or observed vulnerability, and ΔV_m is the sum of behaviour modifier scores provided by the methodology. These modifiers alter the vulnerability index for each building taking specific characteristics into account, such as plan regularity, foundation type, or state of preservation. After calculating $\overline{V}_I$, it is possible to calculate the mean damage grade (μ_D) through the semi-empirical formulation reported in Eq. (10), which correlates the mean damage with the vulnerability for a specified intensity I. This formulation is based on the damage levels derived from the European Macroseismic Scale (EMS-98) [63].

$$\mu_D = 2.5 \cdot \left[1 + \tanh\left(\frac{I + 6.25 \cdot \overline{V}_I - 13.1}{2.3}\right)\right] \tag{10}$$

Furthermore, six damage thresholds (D_k = 0, 1, 2, …, 5) were defined according to the EMS-98 damage scale [63], to get insight into the predicted implications of the present scenario, are: D0 (no damage); D1 (negligible); D2 (moderate); D3 (substantial); D4 (near collapse) and D5 (collapse). These correspond to certain μ_D thresholds as reported in Table 2 [63].

Based on the resulting damages obtained by adopting Eq. (10), the Damage Probability Matrices, DPM (refers to Eq. (11)), were assessed using the weighted average of damages, μ_D, to have an overview of the expected damage [78]:

Table 1
Flood damage levels adopted.

Damage level (DF_k)	Damage type	Damage description	Rainfall water depth [m]
DF0	No damage	No structural or non-structural damage.	$h \leq 0.25$
DF1	Very low	No structural damage, slight non-structural damage.	$0.25 < h \leq 0.5$
DF2	Low	No structural damage, moderate non-structural damage.	$0.5 < h \leq 1.0$
DF3	Moderate	Slight structural damage, moderate non-structural damage	$1.0 < h \leq 1.5$
DF4	High	Moderate structural damage, significant non-structural damage	$1.5 < h \leq 2.5$
DF5	Very high	Significant structural damage, non-structural components destroyed.	$h > 2.5$

Table 2
Earthquake damage levels adopted in the present study.

Damage level (D_k)	Damage type	Damage description	Damage threshold
D0	No damage	No structural or non-structural damage.	$\mu_D \leq 0.5$
D1	Negligible	No structural damage, slight non-structural damage.	$0.5 < \mu_D \leq 1.0$
D2	Moderate	Slight structural damage, moderate non-structural damage.	$1.0 < \mu_D \leq 2.0$
D3	Substantial	Moderate structural damage, heavy non-structural damage	$2.0 < \mu_D \leq 3.0$
D4	Near collapse	Heavy structural damage, very heavy non-structural damage	$3.0 < \mu_D \leq 4.0$
D5	Collapse	Very heavy structural damage	$4.0 < \mu_D \leq 5.0$

$$\begin{cases} p_k = \frac{5!}{k! \cdot (5-k)!} \cdot \left(\frac{\mu_D}{5}\right)^k \cdot \left(1 - \frac{\mu_D}{5}\right)^{5-k} \\ \mu_D = \sum_{k=0}^{5} p_k \cdot k \end{cases} \tag{11}$$

Then, the Risk-UE method allows the assessment in terms of both discrete damage distributions and fragility curves. A beta distribution may be employed to define the damage distribution associated with the investigated building type under consideration, as indicated in the Risk-UE method [75], and given by:

$$p_\beta(x) = \frac{\Gamma(t)}{\Gamma(r) \cdot \Gamma(t-r)} \cdot \frac{(x-a)^{r-1} \cdot (b-x)^{t-r-1}}{(b-a)^{t-1}}, a \le x < b \tag{12}$$

assuming $a = 0$, $b = 6$, $t = 8$ and $r = t\left(0.007\mu_D^3 - 0.052\mu_D^2 + 0.2875\,\mu_D\right)$.

Moreover, Eq. (13) is then used to compute the discrete damage distribution (discrete beta density probability function) using the probabilities associated with damage grades k and k+1, where $k = 0,1,2 \ldots,5$:

$$p_k = P_\beta(k+1) - P_\beta(k) \tag{13}$$

The typological fragility curves, which determine the likelihood of achieving or exceeding a specific damage grade, were obtained directly from the cumulative probability beta distribution as:

$$P\left(D \ge D_K\right) = 1 - P_\beta(k) \tag{14}$$

2.4. Multi-risk assessment

The multi-risk assessment was carried out considering the two risks treated as independent (no interactions). As a result, the total risk analysis may be viewed as the sum of earthquake and flood losses, which may represent the situation in which two different disasters occur in a short period [48].

Because the two hazards discussed here have different processes and metric systems, the risk assessment approach must be consistent for them to be comparable. As mentioned in Ref. [48] the first step is to select a common risk time frame (i.e., the period during which a risk could affect a generic area) and the type of analysis (i.e., probabilistic or scenario-based). The risk time frame, instead, corresponds to the different return periods, which are 2, 5, 10, 20, 50, 100, and 475/500 years, and the effects are evaluated as the total expected losses for each of them.

Furthermore, the same risk metric (i.e. losses) must be adopted for consistent earthquake and flood damage estimates. The losses can be classified as either direct or indirect: direct losses are physical losses, such as physical damage to buildings and infrastructure, as well as casualties and injuries; indirect losses are the result of an indirect impact, such as interruption of functions or disruption of the flow of commerce. As a result, how risk is assessed depends on the hypotheses, although it usually relates to direct losses, further subdivided into economic losses and population losses [30,48,79]. The direct economic losses caused by earthquakes are largely connected to structural damage to buildings, whereas in the event of flooding, damage to contents is more important than structural losses. Furthermore, in the case of a flood event, the consequences in terms of indirect economic losses (interrupted business activities) may be greater than the damage to structures [48]. However, in this study, only direct economic losses related to building structural damages were compared, allowing future research to address risk by including for example content damage, population losses or indirect losses.

The quantification of losses in risk assessment usually results in a risk curve that comes from a fully probabilistic approach. These risk curves, also called Loss Exceedance Curves, LEC, have consequences (i.e. direct economic losses) plotted against the probability of occurrence of the hazard event and, as a result, the area under the curve represents the total risk [48,79]. As a result, a fully probabilistic risk assessment may be produced while considering all probable hazard events as [48]:

$$v(p) = \sum_{i=1}^{\text{Events}} \Pr\left(P > p \middle| \text{Event}_i\right) \cdot F_A\left(\text{Event}_i\right) \tag{15}$$

where $v(p)$ is the exceedance rate of loss p, $F_A(\text{Event}_i)$ is the annual frequency of occurrence of the Event_i, and $\Pr\left(P > p \mid \text{Event}_i\right)$ is the probability of the loss to be greater than or equal to p, conditioned by the occurrence of Event_i. Since the probabilities of exceedance in the loss exceedance curve do not relate to a particular hazard, it is simple and straightforward to compare losses between different hazards [48]. The present research applied two types of curves to compare losses. The first type, known as the Loss Exceedance Curve (LEC), correlates expected losses with the related mean annual frequency of exceedance. The second one, defined as the Probable Maximum Loss curve (PML), relates losses to the return period. Total losses were calculated for both hazards by multiplying the monetary exposure (E_i), as derived by Eq. (3) in Section 2, by the damage level ($D_{\%}$) achieved by the structures in the simulated scenario, i.e. flood $\left(D_{\%}^{FL}\right)$ and earthquake $\left(D_{\%}^{EQ}\right)$. The monetary exposure (E_i) is common between the two hazards, whereas the calculation of damage level varies depending on the analysed hazard.

From the seismic damage ($D_k = 0,1,2, \ldots 5$) evaluated, loss thresholds $\left(D_{\%}^{EQ}\right)$ experienced by the building are taken as provided by Ref. [80]. Accordingly, the index shown in Table 3 represents the correlation between the level of damage and the global damage index, which is comparable to a percentage of the cost of replacement and may be used to estimate economic losses caused by earthquakes.

Flood damage, instead, corresponds directly to the physical damage obtained from the stage-damage curves $\left(D_{\%}^{FL}\right)$. According to Ref. [80], the losses are estimated from the cost of replacement through the global damage index. However, in the current study, the cost of replacement has not been evaluated due to a lack of data, and the market value was used instead. Therefore, the losses are estimated as a percentage of the market value, which represents the decrease in the market value of a building due to a natural event.

3. Results and discussion

3.1. Case study

In the context of a multi-hazard scenario, a thorough vulnerability and risk assessment was conducted for an urban compound situated in the historical city centre of Lisbon. The historical significance of this area is underscored by its vulnerability to various hazards, as evidenced by its exposure to a diverse range of events throughout history (see Section 3.3). The city of Lisbon has a total land area of around 100.1 km^2, with Earth's surface of 86.43 km^2, subdivided into 24 parishes. The population is 548.703 inhabitants (291.224 women and 257.479 men), with a total number of 49.223 buildings, according to the Census data 2021, see Ref. [81]. The case study focuses on the Baixa Pombalina neighbourhood (Fig. 2), which is located in downtown Lisbon between the Rua Nova do Almada (West), Praça Dom Pedro IV and Praça da Figueira (North), Rua da Madalena (Est), and Praça do Comércio (South).

The chosen urban area results from the post-earthquake 1755 reconstruction, which is acknowledged to be vulnerable to several hazards because of its coastal location along the Tagus River and the wide existence of historic masonry structures. The peculiarities of this metropolitan neighbourhood make it a tourist destination representative of the cultural identity of the city and its historic dynamism; and, as a result, it is important to preserve [83]. To demonstrate the significance of the area, the comprehensive heritage conservation plan Plano de Pormenor de Salvaguarda da Baixa Pombalina (PPSBP) was developed in 2011, as detailed in Ref. [52].

The occupancy is mostly mixed, with commercial activity taking place on the ground floor and residential functions taking place on the higher floors [52], see Fig. 3.

The Baixa Pombalina district is one of the most famous places for the Lisbon earthquake of November 1, 1755, because it was destroyed by the disaster, which was followed by a tsunami and fires. Following the tragedy, the destroyed buildings were rebuilt under the leadership of the Marquis of Pombal, and many of the remaining structures were dismantled and rebuilt [52,85,86]. The Pombaline reconstruction was distinguished by the introduction of the so-called building typology “Pombalino”, which was characterised by its robustness, regularity and uniformity [49,52]. These structures marked the introduction of specific structural peculiarities aimed at improving their seismic performance. Indeed, the structural system called the “Pombalino cage”, in Portuguese “Gaiola Pombalina”, consists of a set of internal walls called “frontal” walls, with a three-dimensional timber structure forming a triangular geom-

Table 3
Damage-cost thresholds [80].

Damage level (D_k)	Cost of replacement (%)
D0	0
D1	1
D2	20
D3	40
D4	80
D5	100

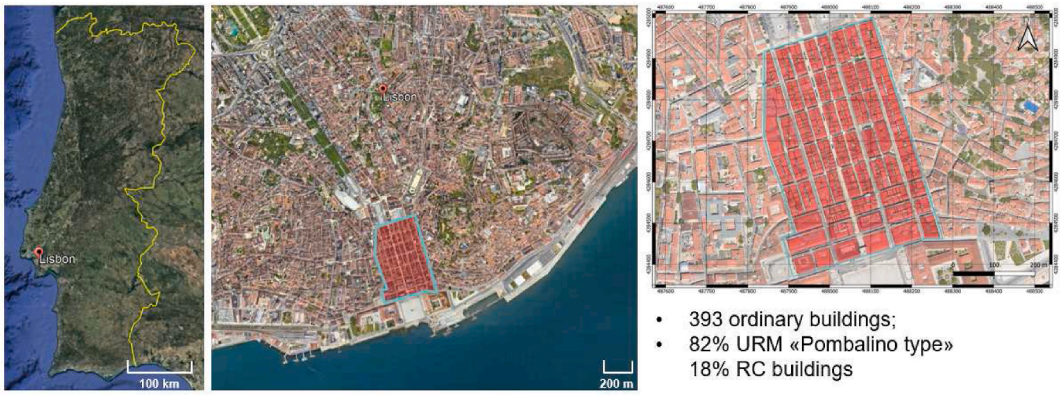

Fig. 2. The case study area: Baixa Pombalina [82].

Fig. 3. Examples of Baixa Pombalina cityscape [84].

etry filled with poor quality masonry, that is connected with the orthogonal walls by vertical studs in the corners. The slabs were formed by wooden beams embedded in the façade and "frontal" walls, with wood planks. Together with the timber floors, the structure ensures the bracing of exterior stone masonry walls and the resistance to forces in any direction [49,52,87].

3.2. Exposure model

The exposure model was developed by compiling a database for the case study area that included multiple building-related attributes such as area, number of floors, typology, position in the aggregate, physical condition and function at the ground floor. In terms of the presence of a basement data were sourced from Ref. [88], indicating that only one ordinary building in the study area includes a basement, and therefore, it was not included in the statistical analysis. These exposure parameters are very important when assessing the physical damage of a building due to a hazard. Indeed, according to Ref. [79], when analysing the degree of damage and possible losses, two types of factors should be defined: the type of negative effects that an event may have on a structure and the building characteristics that determine the degree of damage to a hazard. The negative impacts on a building depend on the type of hazards it faces. These could include things like being hit by falling objects, strong winds, shaking from earthquakes, or flooding, among other possibilities. In each of these situations, the distinctive characteristics of a structure may make it more or less vulnerable to damaging effects [79]. As a result, depending on the hazard type, some features should be examined and evaluated for vulnerability assessment. As an example, during an earthquake, the damage can depend on many factors such as building height (i.e. high masonry buildings are more likely to show high damage [75,89]), location of the building in the aggregate (i.e. intermediate structural units suffer less damage due to the confined behaviour of surrounding cells, whereas corner or head structural units suffer more damage [90]), building typology (i.e. different buildings types will experience different degree of damage [63]) or physical condition (i.e. generally bad condition maintenance increase vulnerability [90]). During a flood event some other characteristics are important, for instance, the building use (that determines the number of people inside the building as well as the type and value of the content [24,91]) or the presence of basement (that can affect the degree of damage even for low levels of water depth [24,91]).

Based on that, a thorough inventory of the examined buildings was assessed, and the findings were subsequently processed in the QGIS tool [51]. The development of a building inventory for the investigated area includes assets potentially vulnerable to a variety of hazards and is an important step in assessing potential losses [14]. This facilitates loss assessment and allows for statistical analysis of the most important building features (see Fig. 4), and spatial visualisation in a GIS environment, as presented in Fig. 5.

Fig. 4 illustrates the statistical analysis of the aforementioned area which, in general terms, contains 393 ordinary buildings constructed in aggregate conditions, with the majority of them being unreinforced masonry (URM – M3.1) "Pombalino" (82 % of the cases) and others built in (RC) reinforced concrete (18 % of the sample) as a result of interventions over the years (Fig. 4a). Regarding the number of floors (Fig. 4b), it is possible to notice that the building's stories vary from 2 to 9 floors, with a significant majority (96 %, i.e. 376 buildings) having from 5 to 7 floors. The physical condition of the buildings (see Fig. 4c) reveals that the majority of them are in good or very good condition (53 % of the sample), while a considerable percentage (42 %) is in moderate to very poor condition. Moreover, it is worth noting that in Fig. 4c, the term "Constr." highlights buildings that were undergoing a restructuring process. Finally, concerning the aggregate conformations (Fig. 4d), which consist of 8 buildings per aggregate on average, present the majority of buildings in the intermediate position (58 %), e.g. enclosed among two internal structural cells within the aggregate, followed by the corner (37 %), e.g. between two buildings in the corner of the aggregate and a lower fraction of buildings categorized as head (5 %) types, at the ends of the aggregate. Finally, in terms of ground-floor building typology, the area under investigation has a large proportion of ground floors (86 % - 340 buildings) allocated to commercial activities, such as shops, hotels and restaurants, with just a small proportion (3 % - 10 buildings) dedicated to residential uses. The remaining buildings (11 % - 43 buildings) were found to be unoccupied, i.e. not in use. Fig. 5 shows maps characterizing the data obtained.

The monetary exposure, for the analysed building sample, is determined by multiplying the floor area of each floor, by the market value, according to Eq. (3) (see Section 2.1). Analysing the [81] database, the market value has been assumed as 5200 €/m^2 for commercial areas and 3788 €/m^2 for residential areas.

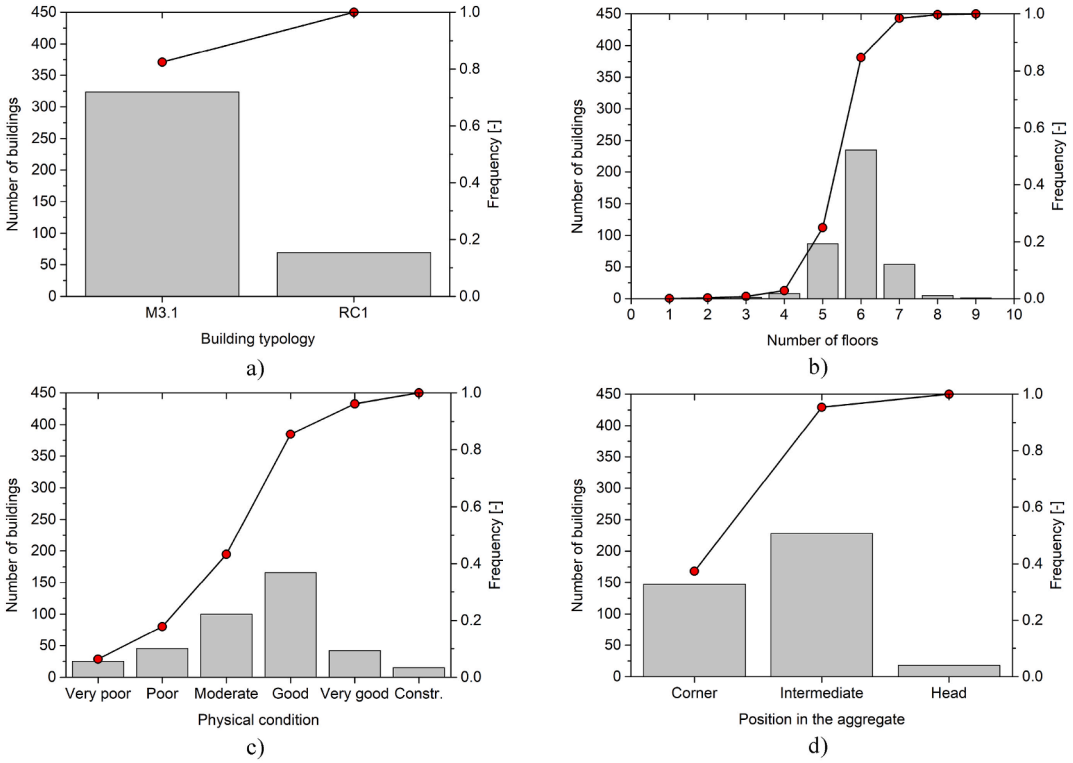

Fig. 4. A statistical representation of main attributes for the study area: a) building typology; b) number of floors; c) physical condition; d) position in the aggregate.

3.3. Hazard model

3.3.1. Flood hazard

Large towns with large populations, such as Lisbon, are often situated on estuaries or next to rivers. Flood assessment is difficult in coastal areas due to the confluence of multiple phenomena, such as tides, river flows, wind, and waves, which are exacerbated by climate change, and Portugal has a relatively high flood risk [92,93]. In the case of Lisbon, the Tagus River estuary covers around 320 km^2 and is surrounded by 18 municipalities of the Lisbon Metropolitan Area (LMA). The LMA has almost three million citizens and is separated into two parts by the estuary: north and south [81,93,94]. In this context, the study in Ref. [94] explains that the Northern LMA, where is located the examined case study building stock, is more vulnerable to pluvial flooding than the Southern LMA due to a higher proportion of built-up areas, smaller drainage basins, a greater extension of low permeability formations, and higher values of average altitude and slope. Lisbon has a long history of experiencing floods with the three most significant flood events being on November 25–26th, 1967, November 18–19th, 1983, and February 18th, 2008 [94]. On November 25–26, 1967, Lisbon experienced the deadliest natural disaster since the devastating earthquake of 1755. Rain with extraordinary intensity fell on the Lisbon metropolitan area, causing flash floods and landslides. The November 1967 event set daily rainfall records (137 mm) that were significantly higher than the normal average for that single month (100 mm). This event had significant socioeconomic consequences: official estimates reported 495 killed people as a result of the floods in Lisbon's densely populated metropolitan area; nearly 900 people lost their homes; and, several road and train communications were disrupted [50,94]. In the same month, but several years later, the Lisbon area witnessed an extraordinary precipitation event on November 18–19th, 1983. This event was swiftly followed by extensive urban flash floods and landslides. The November 1983 event set daily rainfall records (164 mm), higher than the monthly average, making this day the rainiest day in the twentieth century. This high rainfall event resulted in flash floods, urban inundation, and landslides. Despite the lack of official records, the reported overall number of fatalities was ten, with huge economic losses as a result of power outages and obstructed road and rail lines [94,95].

In more recent years, on 18th February 2008, another intense flood struck Lisbon. The event set a daily rainfall record (141 mm) much higher than the normal average for that month (89 mm). This catastrophic event resulted in urban inundation, flash floods, and landslides. The National Authority of Civil Protection reported 4 deaths, 65 individuals displaced, and 121 evacuated. There is no official assessment of the economic damage related to this event, such as rail service disruptions, blocked roads, and power outages [94,96]. Datasets about the precipitation in Lisbon from 1864 to 2018 (i.e. 154 years) are provided by Ref. [97] and the distribution of the recorded daily rainfall data (mm) in Lisbon is reported in Fig. 6, with the average M and limit with ± twice the standard deviation σ.

As outlined in Section 2.2, the current case study exclusively focuses on pluvial floods, while disregarding alluvial floods that may arise from the Tagus River. This assumption relies on data from the Agência Portuguesa do Ambiente [98] in the Planos de Gestão dos Riscos de Inundações (PGRI). The PGRI provide strategies to minimize the negative consequences of flooding in high-risk areas, and it

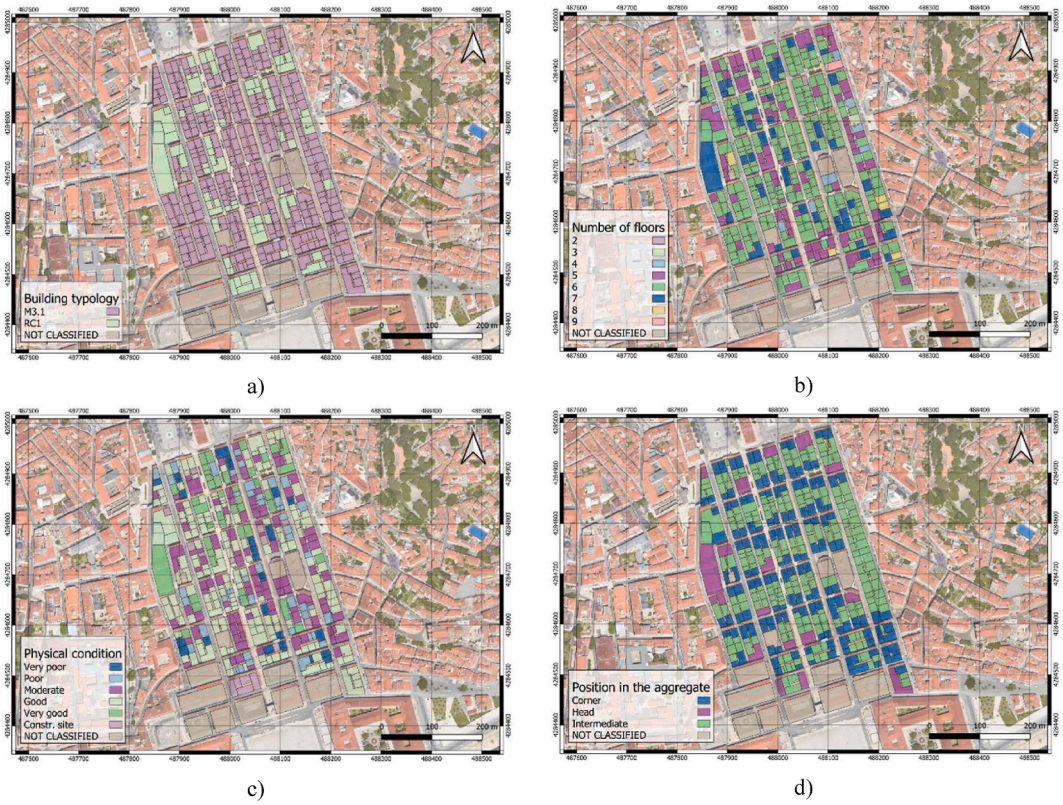

Fig. 5. Spatial representation of main attributes for the study area: a) building typology; b) number of floors; c) physical condition; d) position in the aggregate.

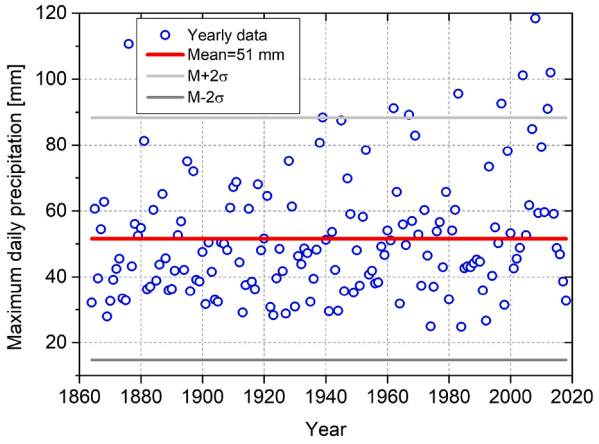

Fig. 6. Distribution of maximum daily precipitation (1864–2018) for Lisbon. Available at https://www.ipma.pt/en/oclima/series.longas/list.jsp.

conforms with "Directive 2007/60/EC of the European Parliament and of the Council of 23 October 2007 on the Assessment and Management of Flood Risks." The PGRI have been evaluated and updated by the Directive's second cycle of implementation (2022–2027) and the mapping of areas of considerable potential flood risk (Áreas de Risco Potential Significativo de Inundação, ARPSI), has been made available, as shown in Fig. 7.

As observed in Fig. 7, the Baixa Pombalina area is not affected by inundation due to the river for any return period (20-100-1000 years), for this reason, the current work specifically analysed the pluvial flood derived from rainfall events. As described in Section 2, the main input data categories required by the HEC-RAS 2D model are topographic data and unsteady flow data. The most important terrain data are the DEM, obtained from the SRTM downloader plugin in QGIS [51], see Fig. 8, and land-use data, obtained from the Esri Land Cover website [57].

For the input data of precipitation, the IDF curves have been used for different return periods (2-5-10-20-50-100-500 years). In the case of Portugal, the IDF curves developed by Ref. [60] have been taken into account. This type of curves, see Fig. 9a, are those that

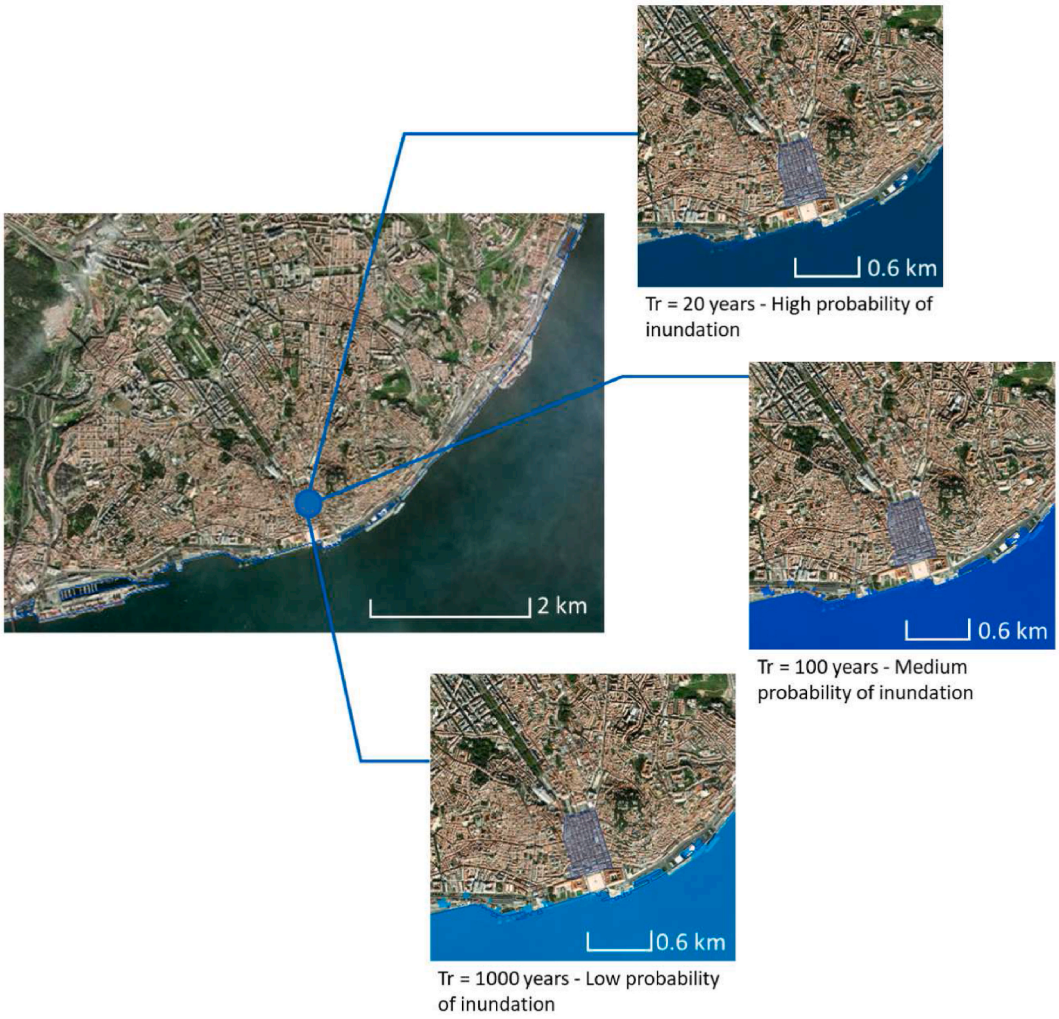

Fig. 7. Flood area due to alluvial flood in Lisbon for 20, 100 and 1000-year return periods. The blue dot indicates the location of the case study area, instead, the filled blue area delineates the boundaries of the investigated urban compound.
Available at https://sniamb.apambiente.pt/content/diretiva60ce2007-2%25C2%25BA-ciclo.

Fig. 8. Digital elevation model, DEM, for Lisbon.

best match the relationship between precipitation intensity and duration for a given return period, for further details see Ref. [60]. The hydrographs were assessed using the SCS-CN method [58], detailed in Section 2.2. Following this, the volumetric flow rate of the hydrographs was transformed into water height (mm) by dividing them by the area of the studied basin (0.501 km^2). The resulting hyetographs are depicted in Fig. 9b.

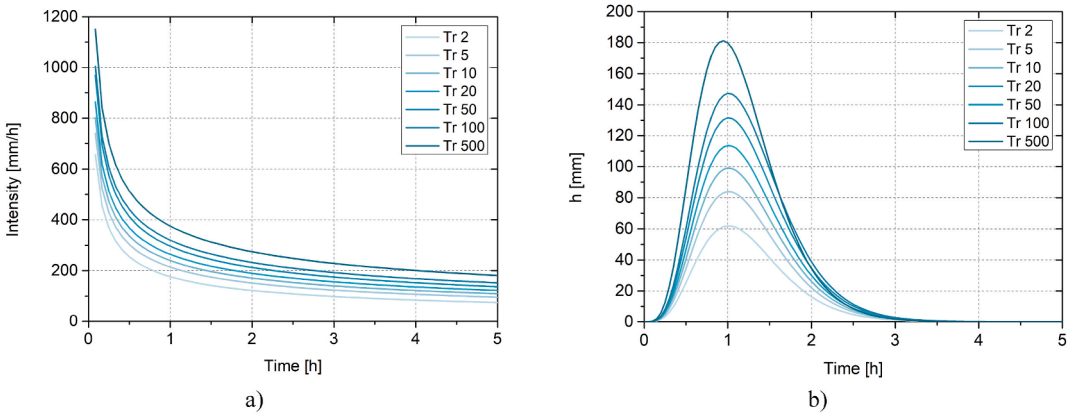

Fig. 9. Precipitation data for Lisbon: a) IDF curves; b) hyetographs.

The hyetographs represent the boundary condition for the rainfall model developed in HEC-RAS software [56], which allowed the simulation of flood depth maps for the return periods adopted, see Fig. 10. It is worth noting that the areas with a water depth over 2.5 m can be attributable to the type of floods that have been simulated, specifically rainfall floods. Indeed, these floods are caused by severe rainfall, which produces a slow increase in the gradient of water levels dependent on the topography of the area, until structures are flooded.

3.3.2. Seismic hazard

The Algarve region (south of Portugal) is considered to have the highest seismic hazard on the Portuguese mainland. Given the exposure and vulnerability, Lisbon is likely to have the highest risk. Portugal's mainland is prone to seismic hazards due to its location on the Eurasian plate near the boundary with the African plate, which primarily results in very large offshore earthquakes and moderate to large onshore earthquakes [49,99]. Earthquakes have struck Portugal, and particularly Lisbon, several times in the past [49]. According to the records, an earthquake of an estimated magnitude between 6.5 and 7.1 struck Lisbon on January 26th, 1531. This event, named the “Lower Tagus Valley earthquake”, caused significant damage in the city downtown and surrounding areas: the earthquake caused widespread devastation in the city, damaging around one-third of the building stock [100,101]. The most significant earthquake in Portugal, with subsequent tsunami and fire events, happened in 1755 on 1st November and is generally referred to as "The Great Lisbon Earthquake", with an estimated magnitude of 8.5–8.7 located offshore. This earthquake destroyed over 85 % of the structures and killed 30,000 to 40,000 people, representing roughly 20 % of the population of Lisbon at the time [49,100]. Due to heavy damage, in the epicentral area, the “Benavente earthquake” (1909) made 80 % of the houses unusable, while 46 people died and 75 suffered injuries. The earthquake mostly devastated the eastern part of Lisbon, where the primary damage in masonry buildings was the partial collapse of chimneys and corners of buildings, as well as vertical cracks. The magnitude of this onshore earthquake, which occurred around 60 km northeast of Lisbon, was 6.0 [49,102]. The most recent significant earthquake to strike Lisbon was the "Algarve earthquake" in 1969, which had a magnitude of 7.8 and was centred offshore to the south of Algarve. This earthquake killed 13 people and mostly struck the south of Portugal, where over 400 structures were seriously damaged, while the primary damage noticed in Lisbon was the collapse of several chimneys [49]. In the last ten years (2013–2023), there have been 96 earthquakes with a magnitude of four or higher that have occurred within 300 km of Portugal, resulting in an average of nine 4+ earthquakes annually; no earthquakes with a magnitude greater than six was recorded (see Fig. 11). This information can be obtained by analysing online datasets about the more recent earthquakes in Portugal [103].

Based on the data acquired from Refs. [99,104], the mean Peak Ground Acceleration (PGA) hazard map for Portugal reveals PGA values spanning from 0.035g to 0.25g in rock. The expected PGA value for the Lisbon Metropolitan Area is 0.2g associated with a 10 % probability of exceedance within a 50-year (i.e. return period of 475 years). Starting from this value, Eq. (7) (see Section 2) has been used to estimate the acceleration for different return periods (T_R), i.e. 2-5-10-20-50-100 years, see Fig. 12a. Subsequently, the PGA has been related to the EMS-98 macroseismic intensity [63] through empirical correlation as explained in Ref. [64] (see Eq. (8) in Section 2) and reported in Fig. 12b.

3.4. Vulnerability model

3.4.1. Flood vulnerability

The present research adopted the stage-damage curves reported by Ref. [88] applied for the same building sample. These curves relate the water depth (in m) with the degree of damage $\left(D_{\%}^{FL}\right)$ ranging from 0 to 100. Moreover, the authors evaluate building damage by categorizing structures based on the presence or absence of a basement, as well as distinguishing between those with two or fewer stories, and those with three or more levels, see Fig. 13. Additionally, it was assumed that the buildings in the case study area were unlikely to suffer any damage at water levels below 0.25 m. Because of the varying ground elevations in the area, this assumption is reasonable; indeed, the above-mentioned threshold indicates the average height of entrance doors over the road level of buildings as suggested by Ref. [24].

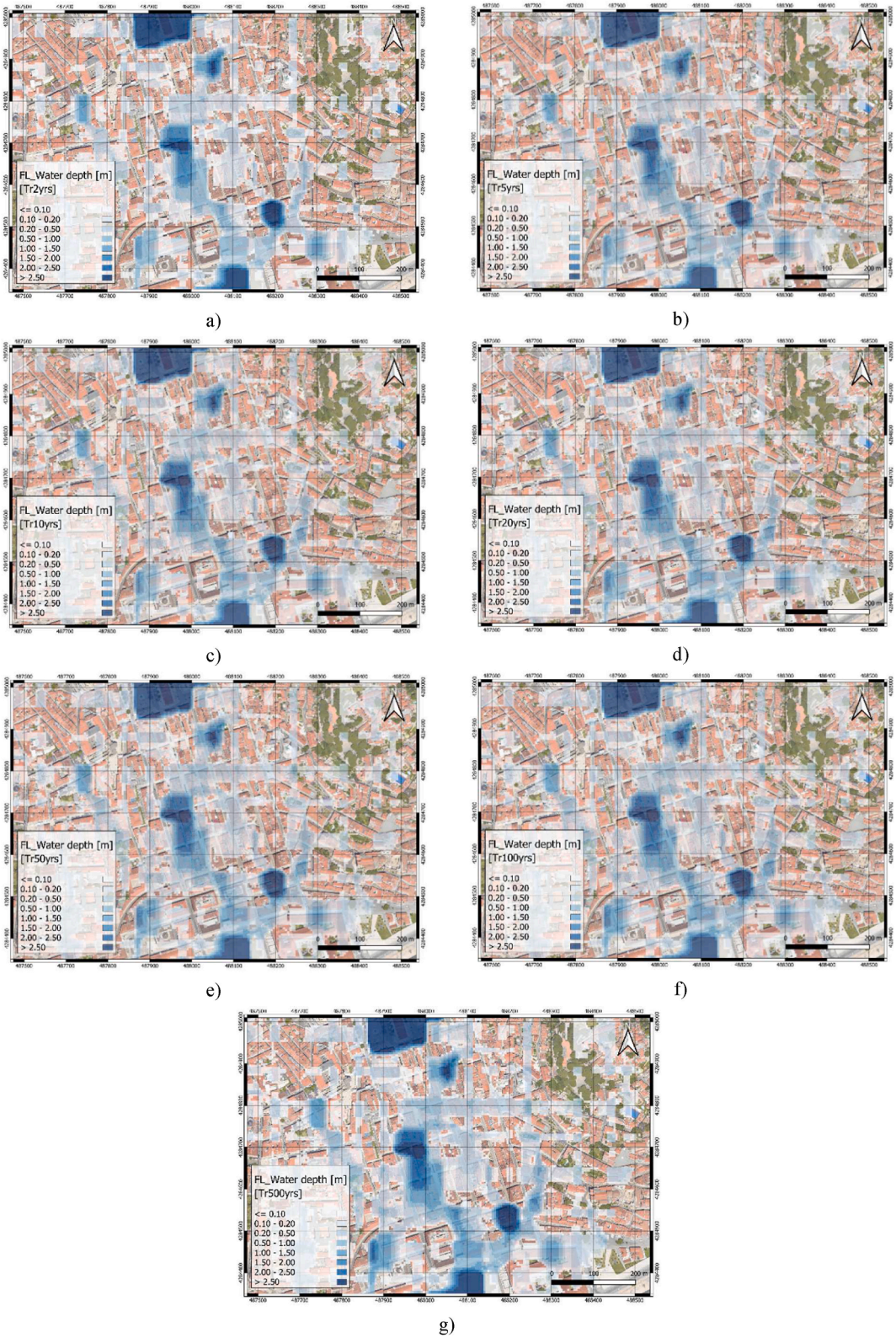

Fig. 10. Pluvial depth maps for: a) 2 years; b) 5 years; c) 10 years; d) 20 years; e) 50 years; f) 100 years and g) 500 years return period.

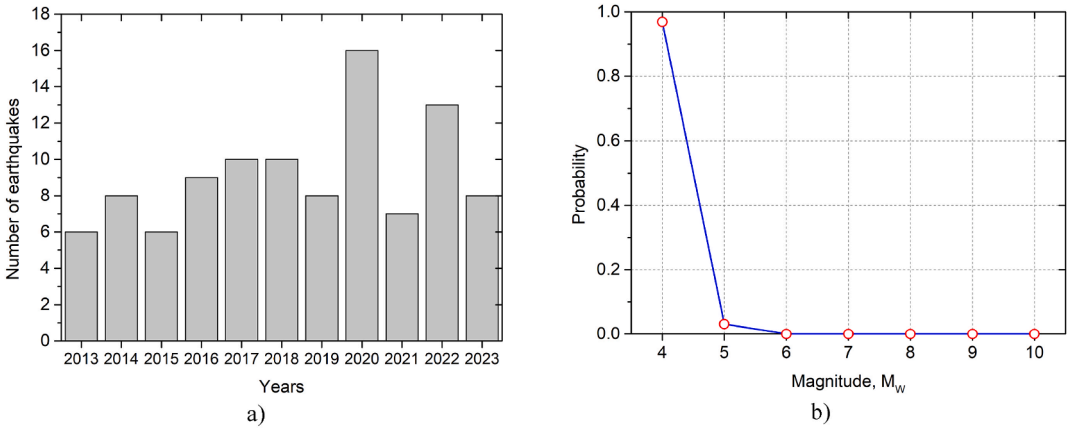

Fig. 11. Analysis of earthquake data (2013–2023) with a magnitude of 4 or higher within 300 km of Portugal: a) number of recorded earthquakes; b) probability distribution of the occurred earthquake. Available at https://earthquakelist.org/portugal/#statistics.

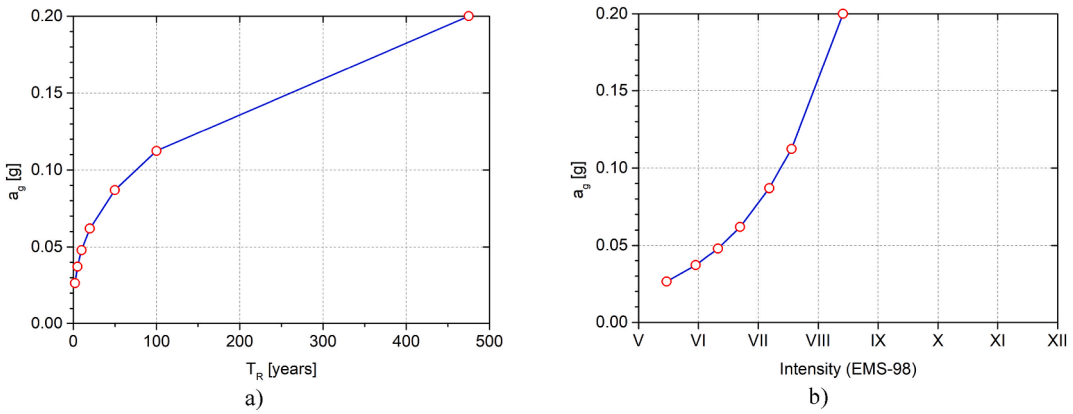

Fig. 12. PGA estimation for the analysed return periods: a) expected PGA values as a function of the return period, T_R; b) correlation between PGA and EMS-98 macroseismic intensity.

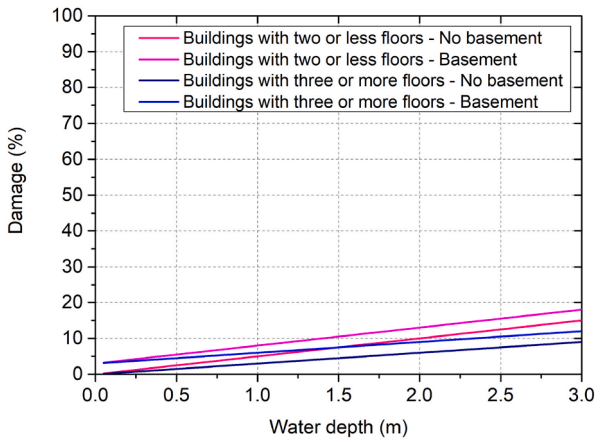

Fig. 13. Adopted Stage-damage curves [88].

Given these stage-damage curves, the flood damage has been calculated through the water level that every building experiences for the associated return period. Six flood damage thresholds have been provided: DF0, DF1, DF2, DF3, DF4, and DF5. These thresholds allowed a simplified visualisation of the damage distribution in the area for the investigated return periods. Here, two scenarios are presented, corresponding to a 2-year and a 500-year return period. These represent the lower and upper limits of the conducted analyses, as reported in Fig. 14.

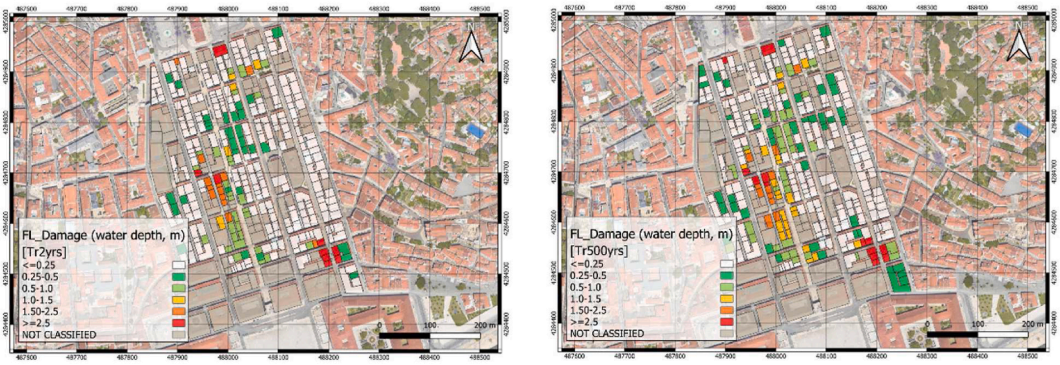

Fig. 14. Flood damage scenarios for: a) 2 years; b) 500-year return periods.

For a return period of 2 years, 73 % of the building sample (i.e. 238 URM buildings) experienced a damage DF0 (water level below 0.25 m), while 3 % of the sample (i.e. 9 buildings) experienced a water depth over 2.50 m (i.e. more than 2.50 m). For a 500-year return period, 61 % of URM buildings had water depths below 0.25 m (DF0), while just 4 % faced depths over 2.50 m (DF5).

3.4.2. Seismic vulnerability

According to the Risk-UE project, the vulnerability index and damage grade for each building have been calculated. Based on the features of the structures, the 324 Pombalino URM buildings of the current study area were analysed and an M3.1 category (i.e. wooden slabs URM) was assigned, to which corresponds a most probable value of the vulnerability index $V_I^* = 0.74$, see Table 4.

Starting from the most probable value of the vulnerability index for the abovementioned category, a series of behaviour modifications have been summed ΔV_m to consider the specific characteristics of each building. In Fig. 15, a spatially vulnerability index distribution is presented.

The results reveal that 75 % of URM buildings have very high vulnerability ($V_I > 0.8$), while 25 % present a V_I between 0.6 and 0.8 (high vulnerability). Then, the mean damage grade (μ_D) has been evaluated through the semi-empirical formulation, see Eq. (10) in Section 2, which correlates the mean damage with the vulnerability index for a specified intensity I. Moreover, the six damage thresholds (D0,.., D5), determined according to the EMS-98 damage scale [63], allowed for the damage-predicted implications for different scenarios. Concerning the above-introduced formulation, it is worth noting that the reason for using the mean damage curve from the literature is that there is no historical record of events that have occurred in Portugal, making calibration difficult. However, this should be investigated further in other case studies characterized by the same structural taxonomy of the buildings present in the case study area. Similarly, Fig. 16 offers a comprehensive overview of the simulated scenario, encompassing the lower and upper bounds (i.e. 2 and 475-year return periods, respectively).

Table 4
Building vulnerability index for M3.1 category [75].

Category (BTM)	$V_{I,BTM}^{min}$	$V_{I,BTM}^{-}$	$V_{I,BTM}^{*}$	$V_{I,BTM}^{+}$	$V_{I,BTM}^{max}$
M3.1 Wooden slabs	0.46	0.65	0.74	0.83	1.02

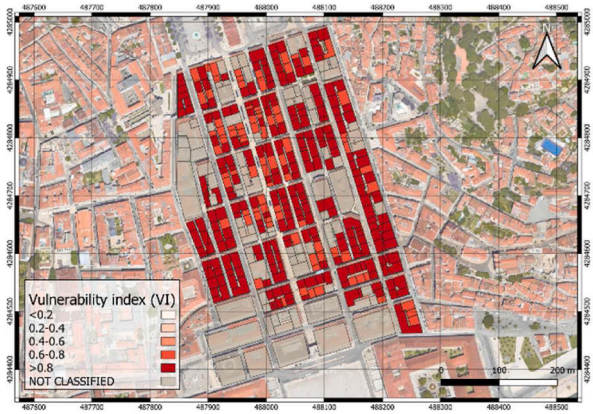

Fig. 15. Spatial vulnerability distribution for Baixa Pombalina.

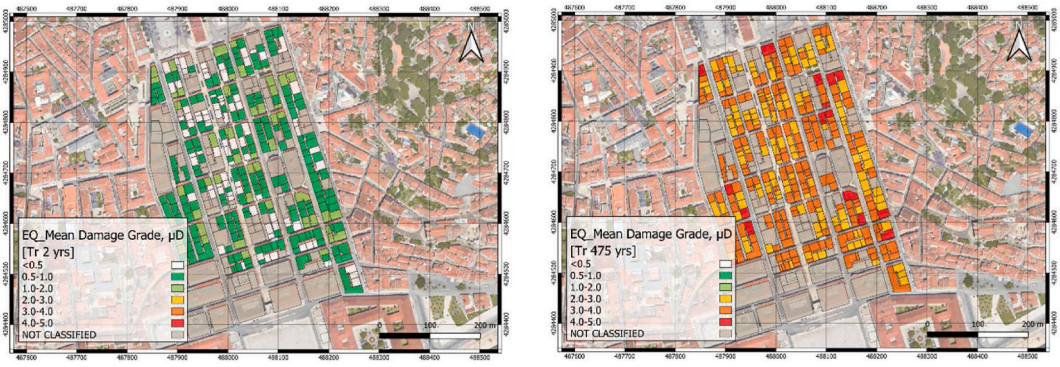

Fig. 16. Earthquake damage maps: a) 2 years; b) 475-year return periods, respectively.

The damage analysis shows for a 2-year return period that 26 % of the buildings experience damage grade D0, 59 % D1, and 15 % D2. For a return period of 475 years, the damage distribution is as follows: 38 % of buildings are classified as D3, 57 % fall into the D4 category, and the remaining 5 % are categorized as D5. Consequently, the Damage Probability Matrices, DPMs, were assessed for each simulated scenario using the weighted average of damages, μ_D, as discussed in Ref. [78]. Moreover, the results for the above-introduced return periods, i.e. 2-year and 475-year, are depicted in Fig. 17.

Finally, the fragility curves as well as discrete damage distributions were calculated for the M3.1 category according to Ref. [75], as shown in Fig. 18. From the results obtained, it is evident that for a 2-year return period, which corresponds to a macroseismic intensity of 5.5, there is a 40 % probability of exceeding damage level D1. In contrast, for a 475-year return period, the seismic intensity increases up to 8.4, resulting in a 100 % probability of exceeding the D1 threshold, a40 % probability of exceeding the D4 threshold, and a 15 % probability of occurrence of the D5 threshold (collapse).

3.5. Multi-risk assessment

The multi-risk assessment was carried out under the assumption of independence between the two hazards, as described in Section 2, with no interactions considered. The overall risk was computed as the sum of earthquake and flood losses, resembling a scenario in which two independent events may occur in a short period [48]. Then, a comprehensive analysis was conducted to examine the relationship between the increase in seismic damage caused by floods, providing a thorough assessment of potential losses in the studied multi-hazard context. The study specifically quantifies the extent to which flood-related losses amplify earthquake losses across the examined return periods. To delve into the details, the study estimates losses for each return period, considering both flood and earthquake hazards. Following this, the total losses were computed by summing up earthquake and flood losses for the same return period, T_R. Consequently, Fig. 19a presents the Multi-Hazard Probable Maximum Losses curve (MHPML). Subsequently, Fig. 19b depicts the Multi-Hazard Loss Exceedance Curve (MHLEC), expressed in terms of annual frequency losses. Finally, Fig. 19c depicts the two independent loss curves associated with the above-mentioned hazards, i.e. pluvial floods and earthquakes. This representation facilitates a more effective comparison of the consequence-loss model presented in Ref. [105].

As expected, for longer return periods, building losses are higher as shown in the multi-hazard curve reported in Fig. 19a. Indeed, for a 2-year return period, earthquake losses are approximately 76 M€ while flood losses are around 14 M€. For a 475/500-year scenario, losses caused by earthquakes are around 1150 M€ and flood losses are around 22 M€. Additionally, Fig. 19c highlights the sig-

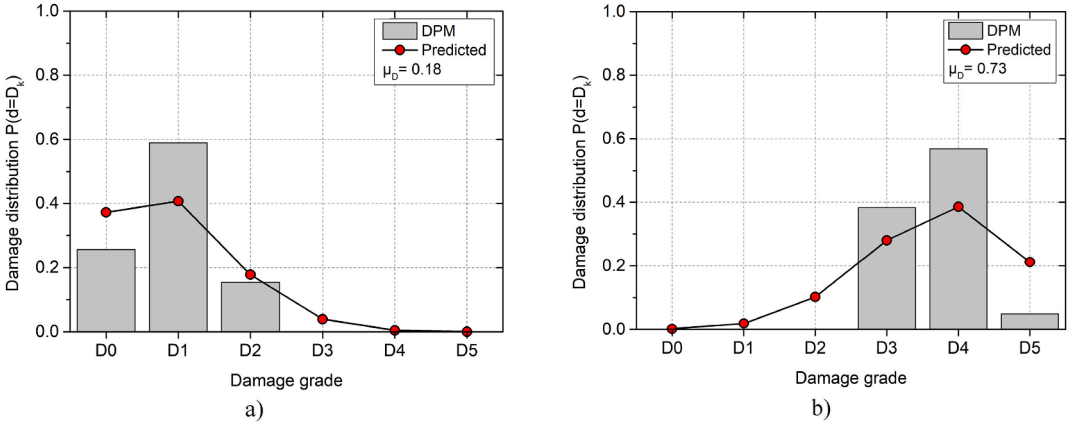

Fig. 17. Damage probability matrices for the analysed return periods: a) 2 years; b) 475 years.

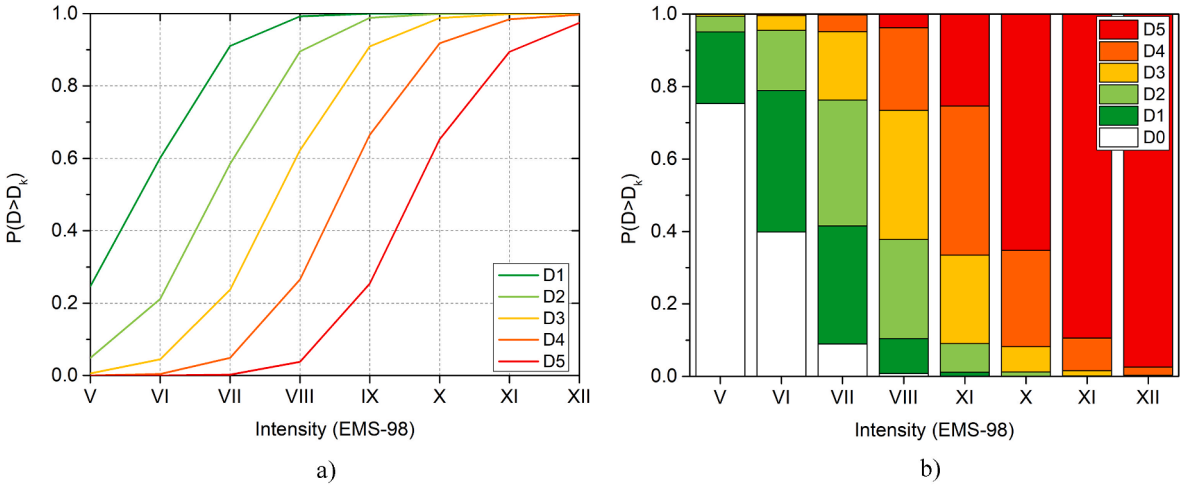

Fig. 18. Vulnerability estimation for M3.1 typology: a) fragility functions; b) discrete damage distribution.

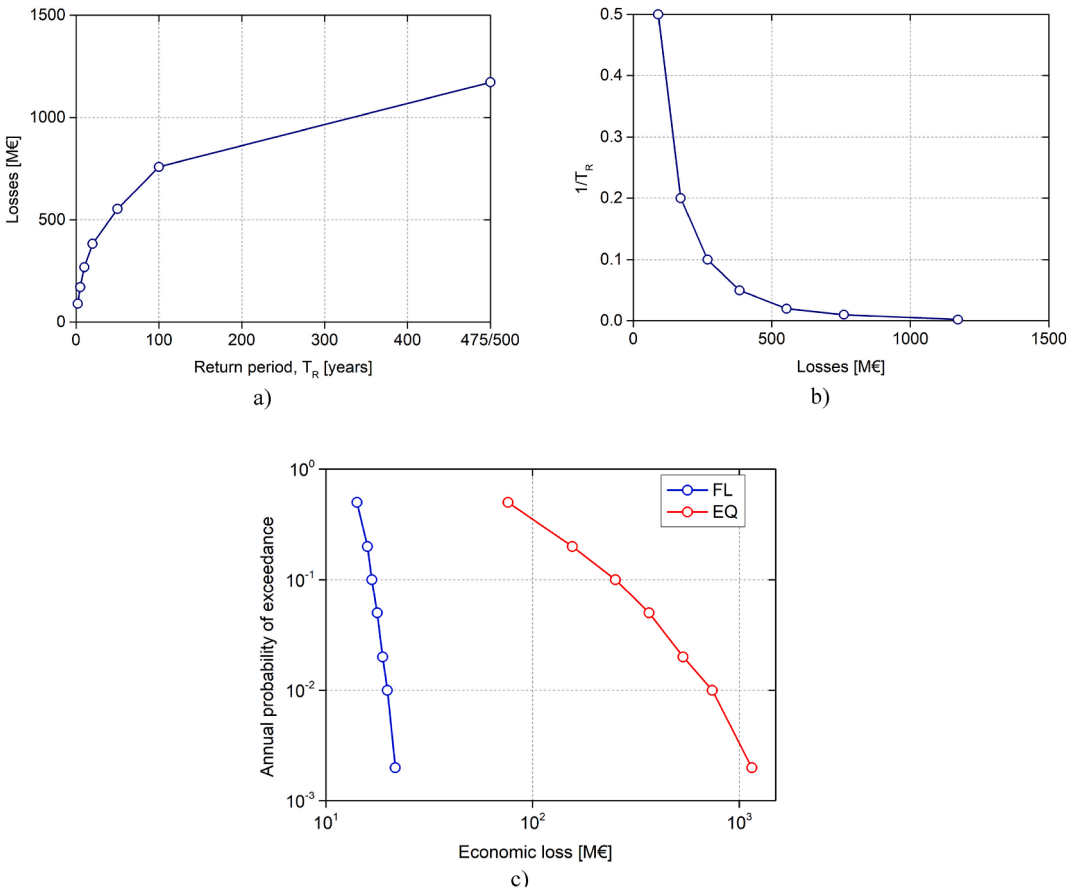

Fig. 19. Multi-Hazard Curves: a) MHPML; b) MHLEC; c) Loss curves for floods and earthquakes.

nificantly higher losses attributed to earthquakes compared to those originating from floods. This contrast in terms of losses can be attributed to the nature of the analysed damages. The resulting loss data are summarized in Table 5. The current work only considers damage to the structure that for an earthquake event has a higher impact compared to the degree of damage caused by floods, which affect the content losses and larger indirect losses.

Next, the relationship between seismic and flood consequences has been calculated. Fig. 20a shows how the flood losses represent a fraction of total losses between 7% and 16 % for return periods of 2, 5, and 10 years when both hazards occur nearby. However, the flood losses only represent between 2% and 5% of total losses for longer return periods (20, 50, 100, 475/500 years). The significantly

Table 5
Evaluated hazard losses.

Return period T_R [years]	Earthquake losses [M€]	Flood losses [M€]
2	76.17	14.13
5	155.63	15.87
10	251.66	16.67
20	366.00	17.71
50	534.74	18.82
100	740.23	19.82
475/500	1150.12	21.65

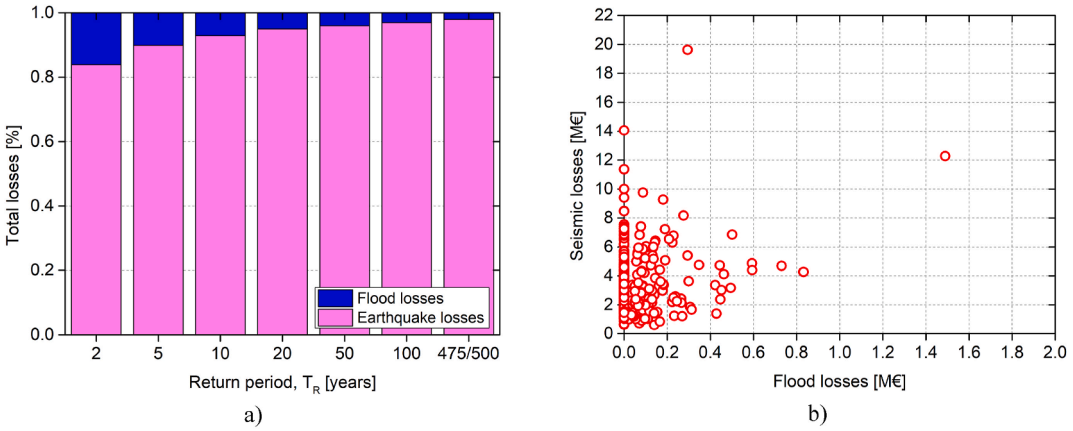

Fig. 20. Estimation of the losses: a) increase of seismic losses due to floods; b) multi-risk correlation.

lower losses induced by floods can be attributed to the fact that, in flood events, only a portion of the building, usually the lower floors, contributes to the overall damage. In contrast, earthquakes involve the entire structure, leading to more widespread damage and consequently higher losses. In Fig. 20b, the multi-risk correlation between earthquake and flood losses is depicted for a return period of 475/500 years, and each analysed building is represented by a red dot. The X-axis represents flood losses, and the Y-axis represents earthquake losses. Notably, seismic losses have a more substantial impact than flood losses, with several buildings experiencing only seismic losses (as indicated by red dots along the Y-axis).

4. Further developments

This study represents a significant advancement in multi-hazard research, in line with established scientific perspectives [1,25,26,106]. Recognizing the need for effective disaster mitigation, the research addresses the limitation of predominantly focusing on single hazards despite the demonstrated geographical and temporal overlap of natural hazards [7,107]. While not explicitly exploring interactions between potential hazards and vulnerabilities, the study allows for ranking and comparing various risks affecting a specific area. By harmonizing assessment procedures and metrics, it provides a valuable tool for prioritizing risk reduction initiatives and tailoring urban risk mitigation strategies. The application of a multi-risk methodology in the city centre of Lisbon, coupled with the estimation of expected economic losses, is a novel approach. Notably, the study's focus on rainfall-induced floods holds particular significance for Lisbon, addressing a commonly experienced phenomenon in the region [50,94–96].

Despite the novelty of the work, it is essential to understand its limits, as they point to future advancements and enhancements to the multi-risk assessment process. Concerning the literature advancement [29,39], the initial limitation lies in the oversight of interrelations between seismic and flood hazards. Placed within multi-layer single-hazard methodologies [4,14], the analysis independently addresses different hazards [29]. To enhance hazard interrelationship, future developments could integrate the probability of occurrence for both events through Multi-Criteria Analysis (MCA), selecting and combining significant parameters of different hazards. In dealing with a multi-hazard perspective, vulnerability dependence is essential [26]. Considering vulnerability to different hazards necessitates accounting for different contributions of the structural building components, hazard consequence variability, and progressive impacts. Overcoming these challenges remains a task for future improvement.

The methodology could be refined by addressing vulnerability changes occurring when two independent hazards overlap spatially and temporally, such as a flood following an earthquake or vice versa. Vulnerability changes can occur when (i) building characteristics influences differently the overall vulnerability level, for example, although they might increase vulnerability to flood, wide windows on the ground floor can reduce fire vulnerability [5,26]; (ii) the impact of many hazards on a structure changes its vulnerability; for example, if the roof is covered with snow or volcanic ash, the impact of an earthquake may be higher because the increased weight alters the structural behaviour of the building [26]; (iii) building vulnerability can be altered by the sequential impact of several hazards since the structure is already compromised after the first hazard, and the effect of the second hit is likely to be greater than in the

case of an undamaged building [26]. Some works have tried to overcome this limitation [43,47], however, this remains a challenging task.

The methodology presented herein could be improved further in this regard by accounting for vulnerability changes that may occur if two independent hazards overlap spatially (the same area) and temporally (one hazard occurs shortly after another), such as when a flood occurs in the aftermath of an earthquake or vice-versa. For example, the impact of a rainstorm event may be greater if the building has already been damaged by the earthquake, or the impact of the earthquake may be greater if a flood event has already occurred, since vulnerability conditions may differ owing to rain infiltration. This can occur, for example, if the roof is severely damaged by the earthquake and rain penetration is permitted through the superior part of the wall. However, water penetration or rising in the walls caused by a flood event can reduce the strength qualities of the structural material and, as a result, have a higher impact if affected by an earthquake.

An insightful research study proposed by Ref. [108] delves into understanding the vulnerability of masonry walls to flash floods in alpine areas. Using a limit analysis framework, the study considers various building configurations and demonstrates stability thresholds as a function of water depth given in dimensionless form. The study acknowledges the influence of debris resulting from seismic events on subsequent flood impacts, known as debris loading (i.e. material can be carried by the water and inflict more damage to structures) [109]. This phenomenon raises significant post-disaster risk management concerns, emphasizing the need for accurate debris categorization, quantification and logistical issues useful for reconstruction plans for the affected areas [110].

While the obtained results provide a reliable preliminary estimate of losses, a more detailed and comprehensive loss estimation is essential for a thorough understanding [24,48]. Future investigations should consider expanding the types of losses evaluated beyond structural damages, particularly in assessing economic and social value in cultural heritage contexts [66,91]. A challenge in monetary assessment arises from a lack of data, with losses estimated as a percentage of market value. The study suggests future interesting progress by comparing losses as market value depreciation with losses estimated as reconstruction cost, considering potential cost increases during post-disaster recovery [111]. Indeed, it must be noted that prices (i.e. reconstruction cost) may increase significantly in the case of an emergency or post-disaster recovery [111]. This approach may be of interest to various stakeholders, including insurance companies and property owners, highlighting the ongoing potential for advancements in multi-risk assessment methodologies.

Finally, in the proposed study, no mitigation strategies for reducing disaster risk have been provided, despite recognizing vulnerabilities and risks. However, future research should focus on developing refined methodologies to reduce losses, enhance community preparedness, and increase urban resilience. In light of these considerations, the current scientific work aims to further provide research initiatives by getting into strategies for completely analysing the several hazards affecting increasingly vulnerable cities. Despite the present contribution, the main goal is to significantly improve the field of multi-risk assessment. The study aims to have an important part in the development and enhancement of risk-reduction techniques to accomplish so by allowing decision-makers and communities to effectively mitigate the negative effects of natural catastrophes.

5. Conclusions

The research work presents a thorough multi-risk assessment model for Lisbon's historic city centre, with an emphasis on seismic and rainfall-induced flood threats. As reported in Refs. [5,24,26], the inherent challenges in multi-disciplinary subjects, diverse metric systems, and distinct process characteristics across hazards highlight the ongoing difficulty in establishing well-defined multi-hazard assessment methodologies, particularly in historic city centres. The study applies the model to Baixa Pombalina, which is highlighted for its unreinforced masonry (URM) structures, to emphasise the relevance of historical urban areas in multi-risk assessment and mitigation. The consideration of earthquakes and rainfall-induced floods as independent hazards reflects a scenario where two different events occur in a short period [48].

The multi-risk procedure involved a thorough examination of hazard, vulnerability, and exposure components. The seismic hazard assessment used EMS-98 macroseismic intensity, whereas the pluvial flood hazard assessment considered water depth and inundation area caused by rainfall events. Recognizing the different kinds of damage processes implicit in each hazard, the multi-risk method uses distinct vulnerability models. The Risk-UE model was adopted to estimate seismic susceptibility, while literature-based stage-damage curves contributed to the assessment of flood vulnerability. An individual exposure model made direct comparisons of expected losses for seismic and flood threats feasible. Monetary exposure was estimated by multiplying the market value by the building floor size, simplifying the loss assessment procedure. The quantitative loss estimating method systematically examined multi-risk scenarios, successfully addressing the intrinsic problem given by multiple metrics associated with independent hazards. This comprehensive methodology considerably contributes to gaining an improved understanding of the multi-risk environment, giving useful insights for informed decision-making and strategic urban planning.

The analysis results for a 475/500-year return period revealed earthquake losses of approximately 1150 M€ and flood losses amounting to around 22 M€. The higher earthquake losses were primarily attributed to a greater proportion of structural damage, in contrast to flood-related losses, which were more associated with content or indirect losses. Notably, in this highly vulnerable area, flood losses were observed to represent 7%–16 % of total losses for return periods of 2, 5, and 10 years when both hazards occurred nearby. However, this fraction was reduced to roughly 2%–5% for longer return periods (20, 50, 100, 475/500 years). The multi-risk analysis reveals that the contributions of the two separate hazards to the estimated consequences are quite different. This is determined not only by the type of hazards under consideration but also by the varying degree of vulnerability displayed by the same structures to different hazards (multi-vulnerability).

The type of structure plays a critical role in the evaluation of vulnerability to earthquakes or floods: the vulnerability to earthquakes appears to be significantly larger than the vulnerability to flood for the buildings sample under consideration (URM, wooden

slabs, with a narrow and long plan shape). Importantly, this analysis emphasizes the critical insight gained from assessing the interplay between flood and earthquake risks, providing valuable information for informed decision-making in disaster management and urban planning, ultimately contributing to enhanced resilience and risk reduction strategies for the studied area.

Despite treating the hazards as independent, this approach offers new insights into multi-risk analysis for urban centres, particularly in exploring spatial correlations and joint probability distributions. The choice to use the same return periods was taken to completely evaluate the two hazards for each specified return period. Nevertheless, it is important to note that floods and earthquakes often have distinct occurrences. Floods, which occur more frequently than earthquakes, are more significant for shorter return periods, but earthquakes become increasingly important for longer ones. This contrast is especially notable for critical historical structures, which, owing to their elevated importance factor, are typically associated with longer return periods due to their social and economic repercussions in the case of collapse. This issue can be evaluated in future work; however, this study sets the stage for future and more detailed risk assessments in Lisbon. It could involve combining different hazards, allowing for fully probabilistic risk analysis, and conducting comprehensive risk assessments. The method described herein provides a well-structured framework for prioritizing future risk reduction efforts and tailoring urban risk mitigation measures. Indeed, urban decision-making processes can rely on this methodology to effectively implement disaster response plans as well as to allocate resources for minimising the potential impacts of future risks, resulting in the reinforcement of community preparedness and resilience.

Specifically, the approach outlined in this research, provides a monetary multi-risk evaluation at the single building level, allowing for a more quantitative cost-benefit analysis of potential mitigation actions [24]. However, it is essential to highlight the study's limitations discussed in Section 4, which have been provided for flood and earthquake hazards, but may also be reflected in the current state of the art regarding multi-hazard assessment.

In conclusion, this work is the first step in analysing the multi-hazard problem in the city of Lisbon due to floods and earthquakes. The research emphasizes the practical benefits of the proposed approach, highlighting its ease of implementation.

This method offers an effective strategy for implementing disaster response plans and allocating resources to minimize potential future impacts. The capacity to conduct a monetary multi-risk evaluation at the single building level enables a more quantitative cost-benefit analysis of potential mitigation actions, reinforcing the community's preparedness and resilience.

CRediT authorship contribution statement

G. Mascheri: Writing – original draft, Investigation, Formal analysis. **N. Chieffo:** Writing – review & editing, Supervision, Methodology, Conceptualization. **C. Arrighi:** Writing – review & editing. **C. Del Gaudio:** Writing – review & editing. **P.B. Lourenco:** Writing – review & editing, Supervision.

Declaration of competing interest

The authors declare that they have no known competing financial interests or personal relationships that could have appeared to influence the work reported in this paper.

Data availability

The data that has been used is confidential.

Acknowledgements

This work was partly financed by FCT/MCTES through national funds (PIDDAC) under the R&D Unit Institute for Sustainability and Innovation in Structural Engineering (ISISE), under reference UIDB/04029/2020 (doi.org/10.54499/UIDB/04029/2020), and under the Associate Laboratory Advanced Production and Intelligent Systems ARISE under reference LA/P/0112/2020.

This work is financed by national funds through FCT – Foundation for Science and Technology, under grant agreement 2023.03899.BDANA attributed to the 1th author.

References

[1] V. Gallina, S. Torresan, A. Critto, A. Sperotto, T. Glade, A. Marcomini, A review of multi-risk methodologies for natural hazards: consequences and challenges for a climate change impact assessment, J. Environ. Manag. 168 (2016) 123–132, https://doi.org/10.1016/j.jenvman.2015.11.011.

[2] G. Berz, et al., World map of natural hazards–a global view of the distribution and intensity of significant exposures, Nat. Hazards 23 (2001) 443–465, https://doi.org/10.1023/A:1011193724026.

[3] S. Javadinejad, et al., Relationship between climate change, natural disaster, and resilience in rural and urban societies, in: W. Leal Filho (Ed.), Handbook of Climate Change Resilience, Springer, Cham, 2019, pp. 1–25 https://doi.org/10.1007/978-3-319-71025-9_189-1 [Online]. Available:

[4] K. Johnson, Y. Depietri, M. Breil, Multi-hazard risk assessment of two Hong Kong districts, Int. J. Disaster Risk Reduc. 19 (2016) 311–323, https://doi.org/10.1016/j.ijdrr.2016.08.023.

[5] P.B. Julià, T.M. Ferreira, From single-to multi-hazard vulnerability and risk in Historic Urban Areas: a literature review, Nat. Hazards 108 (2021) 93–128, https://doi.org/10.1007/s11069-021-04734-5.

[6] E. Sesana, A.S. Gagnon, C. Bertolin, J. Hughes, Adapting cultural heritage to climate change risks: perspectives of cultural heritage experts in Europe, Geosciences 8 (8) (2018) 305, https://doi.org/10.3390/geosciences8080305.

[7] M. Dilley, et al., Natural Disaster Hotspots: A Global Risk Analysis, 5, The World Bank Hazard Management Unit, Washington, DC, USA, 2005 [Online]. Available: https://documents1.worldbank.org/curated/en/621711468175150317/pdf/344230PAPER0Na101official0use0only1.pdf.

[8] UNISDR, Sendai framework for disaster risk reduction 2015–2030, Presented at the Proceedings of the 3rd United Nations World Conference on DRR, Sendai, Japan, Geneva: United Nations Office for Disaster Risk Reduction, 2015 [Online]. Available: https://www.unisdr.org/files/43291_sendaiframeworkfordrren.pdf.

[9] UNISDR, Economic Losses, poverty and disasters 1998–2017 [Online]. Available: https://www.unisdr.org/2016/iddr/IDDR2018_Economic%20Losses.pdf, 2018.
[10] I. Pavlova, A. Makarigakis, T. Depret, V. Jomelli, Global overview of the geological hazard exposure and disaster risk awareness at world heritage sites, J. Cult. Herit. 28 (2017) 151–157, https://doi.org/10.1016/j.culher.2015.11.001.
[11] G. Lollino, C. Audisio, UNESCO World Heritage sites in Italy affected by geological problems, specifically landslide and flood hazard, Landslides 3 (2006) 311–321, https://doi.org/10.1007/s10346-006-0059-7.
[12] UNISDR, Hyogo framework for action 2005–2015: building the resilience of nations and communities to disasters. Presented at the Extract from the Final Report of the World Conference on Disaster Reduction (A/CONF. 206/6), the United Nations International Strategy for Disaster Reduction Geneva, 2005 [Online]. Available: https://www.unisdr.org/2005/wcdr/intergover/official-doc/L-docs/Hyogo-framework-for-action-english.pdf.
[13] UNISDR, Terminology on disaster risk reduction, Geneva Switz. www.unisdr.org/files/7817_UNISDRTerminologyEnglish.pdf, 2009.
[14] G. Grunthal, A.H. Thieken, J. Schwarz, K.S. Radtke, A. Smolka, B. Merz, Comparative risk assessments for the city of Cologne–storms, floods, earthquakes, Nat. Hazards 38 (2006) 21–44, https://doi.org/10.1007/s11069-005-8598-0.
[15] UN, Report of the Open-Ended Intergovernmental Expert Working Group on Indicators and Terminology Relating to Disaster Risk Reduction, A/71/644, United Nations General Assembly, 2016. https://www.undrr.org/publication/report-open-ended-intergovernmental-expert-working-group-indicators-and-terminology.
[16] J. Birkmann, Risk and vulnerability indicators at different scales: applicability, usefulness and policy implications, Environ. Hazards 7 (1) (2007) 20–31, https://doi.org/10.1016/j.envhaz.2007.04.002.
[17] S. Sterlacchini, et al., Methods for the characterization of the vulnerability of elements at risk, in: T. Van Asch, J. Corominas, S. Greiving, J.P. Malet, S. Sterlacchini (Eds.), Mountain Risks: from Prediction to Management and Governance, Advances in Natural and Technological Hazards Research, vol. 34, Springer, Dordrecht, 2014, pp. 233–273 https://doi.org/10.1007/978-94-007-6769-0_8 [Online]. Available:
[18] O.D. Cardona, The need for rethinking the concepts of vulnerability and risk from a holistic perspective: a necessary review and criticism for effective risk management, in: G. Bankoff, G. Frerk, D. Hillhorst (Eds.), Mapping Vulnerability: Disasters, Development and People, Earthscan Publishers, London, UK, 2004, pp. 37–51.
[19] Ante Ivčević, Hubert Mazurek, Lionel Siame, Abdelkhalak Ben Moussa, Olivier Bellier, Indicators in risk management: Are they a user-friendly interface between natural hazards and societal responses? Challenges and opportunities after UN Sendai conference in 2015, International Journal of Disaster Risk Reduction 41 (2019). 101301. https://doi.org/10.1016/j.ijdrr.2019.101301. ISSN 2212-4209.
[20] C. Vogel, K. O'Brien, Vulnerability and global environmental change: rhetoric and reality, Bull. Glob. Environ. Change Hum. Secur. 13 (2004) 1–8.
[21] S. De Angeli, B.D. Malamud, L. Rossi, F.E. Taylor, E. Trasforini, R. Rudari, A multi-hazard framework for spatial-temporal impact analysis, Int. J. Disaster Risk Reduc. 73 (2022) 102829, https://doi.org/10.1016/j.ijdrr.2022.102829.
[22] M.-L. Carreño, O.D. Cardona, A.H. Barbat, Urban seismic risk evaluation: a holistic approach, Nat. Hazards 40 (2007) 137–172, https://doi.org/10.1007/s11069-006-0008-8.
[23] A. Tilloy, B.D. Malamud, H. Winter, A. Joly-Laugel, A review of quantification methodologies for multi-hazard interrelationships, Earth Sci. Rev. 196 (2019) 102881, https://doi.org/10.1016/j.earscirev.2019.102881.
[24] C. Arrighi, et al., Multi-risk assessment in a historical city, Nat. Hazards 119 (2023) 1041–1072, https://doi.org/10.1007/s11069-021-05125-6.
[25] R. Ciurean, J. Gill, H.J. Reeves, S. O'Grady, T. Aldridge, Review of Multi-Hazards Research and Risk Assessments, Open Report OR/18/057, British Geological Survey, Nottingham, UK, 2018. https://nora.nerc.ac.uk/id/eprint/524399.
[26] M.S. Kappes, M. Keiler, K. Von Elverfeldt, T. Glade, Challenges of analyzing multi-hazard risk: a review, Nat. Hazards 64 (2012) 1925–1958, https://doi.org/10.1007/s11069-012-0294-2.
[27] UNEP, AGENDA 21, U. N. Conf. Environ. Dev. 3 14 June 1992 Rio Janerio Braz. 1355 U. N. Environ. Programme 1992 (1992) [Online]. Available: https://sustainabledevelopment.un.org/content/documents/Agenda21.pdf.
[28] UN, Report of the world summit on sustainable development, 26 August - 4 September 2002, Johannesburg, South Africa, United Nations, 2002. https://digitallibrary.un.org/record/478154, 2002.
[29] J.C. Gill, B.D. Malamud, Hazard interactions and interaction networks (cascades) within multi-hazard methodologies, Earth Syst. Dyn. 7 (3) (2016) 659–679, https://doi.org/10.5194/esd-7-659-2016.
[30] C.J. Van Westen, S. Greiving, Multi-hazard risk assessment and decision making, in: N.R. Dalezios (Ed.), Environmental Hazards Methodologies for Risk Assessment and Management, IWA Publishing, London, 2017, pp. 31–94 https://doi.org/10.2166/9781780407135 [Online]. Available:
[31] T. De Pippo, C. Donadio, M. Pennetta, C. Petrosino, F. Terlizzi, A. Valente, Coastal hazard assessment and mapping in Northern Campania, Italy, Geomorphology 97 (3–4) (2008) 451–466, https://doi.org/10.1016/j.geomorph.2007.08.015.
[32] A. Karatzetzou, S. Stefanidis, S. Stefanidou, G. Tsinidis, D. Pitilakis, Unified hazard models for risk assessment of transportation networks in a multi-hazard environment, Int. J. Disaster Risk Reduc. 75 (2022) 102960, https://doi.org/10.1016/j.ijdrr.2022.102960.
[33] L. Rosendahl Appelquist, K. Halsnæs, The Coastal Hazard Wheel system for coastal multi-hazard assessment & management in a changing climate, J. Coast Conserv. 19 (2015) 157–179, https://doi.org/10.1007/s11852-015-0379-7.
[34] D. Araya-Muñoz, M.J. Metzger, N. Stuart, A.M.W. Wilson, D. Carvajal, A spatial fuzzy logic approach to urban multi-hazard impact assessment in Concepción, Chile, Sci. Total Environ. 576 (2017) 508–519, https://doi.org/10.1016/j.scitotenv.2016.10.077.
[35] E. Furlan, S. Torresan, A. Critto, A. Marcomini, Spatially explicit risk approach for multi-hazard assessment and management in marine environment: the case study of the Adriatic Sea, Sci. Total Environ. 618 (2018) 1008–1023, https://doi.org/10.1016/j.scitotenv.2017.09.076.
[36] M. Neri, G. Le Cozannet, P. Thierry, C. Bignami, J. Ruch, A method for multi-hazard mapping in poorly known volcanic areas: an example from Kanlaon (Philippines), Nat. Hazards Earth Syst. Sci. 13 (8) (2013) 1929–1943, https://doi.org/10.5194/nhess-13-1929-2013.
[37] E. Pilone, M. Demichela, A semi-quantitative methodology to evaluate the main local territorial risks and their interactions, Land Use Pol. 77 (2018) 143–154, https://doi.org/10.1016/j.landusepol.2018.05.027.
[38] H.X. Chen, S. Zhang, M. Peng, L.M. Zhang, A physically-based multi-hazard risk assessment platform for regional rainfall-induced slope failures and debris flows, Eng. Geol. 203 (2016) 15–29, https://doi.org/10.1016/j.enggeo.2015.12.009.
[39] T. Nishino, Probabilistic urban cascading multi-hazard risk assessment methodology for ground shaking and post-earthquake fires, Nat. Hazards 116 (2023) 3165–3200, https://doi.org/10.1007/s11069-022-05802-0.
[40] G. Barrantes, Multi-hazard model for developing countries, Nat. Hazards 92 (2018) 1081–1095, https://doi.org/10.1007/s11069-018-3239-6.
[41] Z.E.A. El Morjani, S. Ebener, J. Boos, E. Abdel Ghaffar, A. Musani, Modelling the spatial distribution of five natural hazards in the context of the WHO/EMRO Atlas of Disaster Risk as a step towards the reduction of the health impact related to disasters, Int. J. Health Geogr. 6 (2007) 8, https://doi.org/10.1186/1476-072X-6-8.
[42] R.S. Mahendra, P.C. Mohanty, T. Srinivasa Kumar, S.S.C. Shenoi, S.R. Nayak, Coastal multi-hazard vulnerability mapping: a case study along the Coast of Nellore District, East coast of India, Ital. J, Rem. Sens. 42 (3) (2010) 67–76.
[43] K.H. Lee, D.V. Rosowsky, Fragility analysis of woodframe buildings considering combined snow and earthquake loading, Struct. Saf. 28 (3) (2006) 289–303, https://doi.org/10.1016/j.strusafe.2005.08.002.
[44] H. Li, Y. Liu, C. Li, X.W. Zheng, Multihazard fragility assessment of steel-concrete composite frame structures with buckling-restrained braces subjected to combined earthquake and wind, Struct. Des. Tall Special Build. 29 (11) (2020) e1746, https://doi.org/10.1002/tal.1746.
[45] C. Petrone, T. Rossetto, M. Baiguera, C. De la Barra Bustamante, I. Ioannou, Fragility functions for a reinforced concrete structure subjected to earthquake and tsunami in sequence, Eng. Struct. 205 (2020) 110120, https://doi.org/10.1016/j.engstruct.2019.110120.
[46] J.-G. Xu, G. Wu, D.-C. Feng, J.-J. Fan, Probabilistic multi-hazard fragility analysis of RC bridges under earthquake-tsunami sequential events, Eng. Struct. 238 (2021) 112250, https://doi.org/10.1016/j.engstruct.2021.112250.
[47] G. Zuccaro, F. Cacace, R.J.S. Spence, P.J. Baxter, Impact of explosive eruption scenarios at Vesuvius, J. Volcanol. Geoth. Res. 178 (3) (2008) 416–453, https://doi.org/10.1016/j.jvolgeores.2008.01.005.

[48] G. Tocchi, D. Ottonelli, N. Rebora, M. Polese, Multi-risk assessment in the Veneto region: an approach to rank seismic and flood risk, Sustainability 15 (16) (2023) 12458, https://doi.org/10.3390/su151612458.
[49] V. Bernardo, R. Sousa, P. Candeias, A. Costa, A. Campos Costa, Historic appraisal review and geometric characterization of old masonry buildings in Lisbon for seismic risk assessment, Int. J. Architect. Herit. 16 (12) (2021) 1921–1941, https://doi.org/10.1080/15583058.2021.1918287.
[50] R.M. Trigo, C. Ramos, S.S. Pereira, A.M. Ramos, J.L. Zêzere, M.L.R. Liberato, The deadliest storm of the 20th century striking Portugal: flood impacts and atmospheric circulation, J. Hydrol. 541 (2016) 597–610, https://doi.org/10.1016/j.jhydrol.2015.10.036.
[51] A. Graser, Learning QGIS 2.0, Packt Publishing Ltd, 2013.
[52] L. Barchetta, E. Petrucci, V. Xavier, R. Bento, A simplified framework for historic cities to define strategies aimed at implementing resilience skills: the case of Lisbon downtown, Buildings 13 (1) (2023) 130, https://doi.org/10.3390/buildings13010130.
[53] G.M. Calvi, R. Pinho, G. Magenes, J.J. Bommer, L.F. Restrepo-Vélez, H. Crowley, Development of seismic vulnerability assessment methodologies over the past 30 years, ISET J. Earthq. Technol. 43 (3) (2004) 75–104.
[54] S. Giovinazzi, S. Lagomarsino, A macroseismic method for the vulnerability assessment of buildings, Vancouver, BC, Canada, in: Proceeding of the 13th World Conference on Earthquake Engineering, 2004.
[55] G.P. Cimellaro, S. Marasco, Introduction to dynamics of structures and earthquake engineering, vol. 45, in: Geotechnical, Geological, and Earthquake Engineering, vol. 45, Springer, 2018 https://doi.org/10.1007/978-3-319-72541-3 [Online]. Available:
[56] Hydrologic Engineering Center, HEC-RAS 2D Modeling User's Manual, U.S. Army Corps of Engineers, Davis CA., 2021.
[57] Esri Land Cover, [Online]. Available: https://livingatlas.arcgis.com/landcover/(accessed July 2023).
[58] SCS, Hydrology, National Engineering Handbook, USDA, Washington, D.C., 1993.
[59] S.K. Mishra, R.P. Pandey, M.K. Jain, V.P. Singh, A rain duration and modified AMC-dependent SCS-CN procedure for long duration rainfall-runoff events, Water Resour. Manag. 22 (2008) 861–876, https://doi.org/10.1007/s11269-007-9196-6.
[60] C. Brandão, R. Rodrigues, J.P. Costa, Análise de fenómenos extremos precipitações intensas em Portugal continental, Dir. Serviços Recur. Hıdricos Inst. Água Lisb [Online]. Available: https://snirh.apambiente.pt/snirh/download/relatorios/relatorio_prec_intensa.pdf, 2001.
[61] M. Revrenna, Simulazione di due eventi di piena nel bacino del torrente Posina (autunno 2010 e 2012), Bachelor's Degree, University of Padua, 2014.
[62] R.H. McCuen, Hydrologic Analysis and Design, second ed., Prentice Hall, New Jersey, 1998 Englewood Cliffs.
[63] G. Grünthal, European Macroseismic Scale 1998, European Seismological Commission (ESC), 1998.
[64] N. Lantada, L.G. Pujades, A.H. Barbat, Earthquake risk scenarios in urban areas: a review with applications to the Ciutat Vella District in Barcelona, Spain, Int. J. Architect. Herit. 12 (7–8) (2018) 1112–1130, https://doi.org/10.1080/15583058.2018.1503367.
[65] C. Arrighi, B. Mazzanti, F. Pistone, F. Castelli, Empirical flash flood vulnerability functions for residential buildings, SN Appl. Sci. 2 (2020) 904, https://doi.org/10.1007/s42452-020-2696-1.
[66] F. Carisi, K. Schröter, A. Domeneghetti, H. Kreibich, A. Castellarin, Development and assessment of uni-and multivariable flood loss models for Emilia-Romagna (Italy), Nat. Hazards Earth Syst. Sci. 18 (7) (2018) 2057–2079, https://doi.org/10.5194/nhess-18-2057-2018.
[67] T. Tomiczek, A. Kennedy, Y. Zhang, M. Owensby, M.E. Hope, N. Lin, A. Flory, Hurricane damage classification methodology and fragility functions derived from Hurricane Sandy's effects in coastal New Jersey, J. Waterw. Port, Coast. Ocean Eng. 143 (5) (2017) 04017027, https://doi.org/10.1061/(ASCE)WW.1943-5460.0000409.
[68] P.A. Korswagen, S.N. Jonkman, K. Terwel, Probabilistic assessment of structural damage from coupled multi-hazards, Struct. Saf. 76 (2019) 135–148, https://doi.org/10.1016/j.strusafe.2018.08.001.
[69] S. Reese, B.A. Bradley, J. Bind, G. Smart, W. Power, J. Sturman, Empirical building fragilities from observed damage in the 2009 South Pacific tsunami, Earth Sci. Rev. 107 (1–2) (2011) 156–173, https://doi.org/10.1016/j.earscirev.2011.01.009.
[70] R. Paulik, A. Gusman, J.H. Williams, G.M. Pratama, S. Lin, A. Prawirabhakti, K. Sulendra, M.Y. Zachari, Z.E.D. Fortuna, N.B.P. Layuk, N.W.I. Suwarni, Tsunami hazard and built environment damage observations from Palu City after the September 28 2018 Sulawesi earthquake and tsunami, Pure Appl. Geophys. 176 (2019) 3305–3321, https://doi.org/10.1007/s00024-019-02254-9.
[71] C.J. Friedland, Residential building damage from hurricane storm surge: proposed methodologies to describe. Assess and Model Building Damage [Ph.D. Thesis], Louisiana State University, 2009.
[72] S. Xian, N. Lin, A. Hatzikyriakou, Storm surge damage to residential areas: a quantitative analysis for Hurricane Sandy in comparison with FEMA flood map, Nat. Hazards 79 (2015) 1867–1888, https://doi.org/10.1007/s11069-015-1937-x.
[73] O.M. Nofal, J.W. van de Lindt, Minimal building flood fragility and loss function portfolio for resilience analysis at the community level, Water 12 (8) (2020) 2277, https://doi.org/10.3390/w12082277.
[74] O.M. Nofal, J.W. van de Lindt, T.Q. Do, Multi-variate and single-variable flood fragility and loss approaches for buildings, Reliab. Eng. Syst. Saf. 202 (2020) 106971, https://doi.org/10.1016/j.ress.2020.106971.
[75] Z.V. Milutinovic, G.S. Trendafiloski, Risk-UE an advanced approach to earthquake risk scenarios with applications to different European towns, Contract EVK4-CT-2000-00014 WP4 Vulnerability Curr, Build (2003) 1–111.
[76] A. Aguilar-Meléndez, L.G. Pujades, A.H. Barbat, M.G. Ordaz, J. de la Puente, N. Lantada, H.E. Rodríguez-Lozoya, A probabilistic approach for seismic risk assessment based on vulnerability functions. Application to Barcelona, Bull. Earthq. Eng. 17 (2019) 1863–1890, https://doi.org/10.1007/s10518-018-0516-4.
[77] M.M. Kassem, F.M. Nazri, E.N. Farsangi, The seismic vulnerability assessment methodologies: a state-of-the-art review, Ain Shams Eng. J. 11 (4) (2020) 849–864, https://doi.org/10.1016/j.asej.2020.04.001.
[78] S. Lagomarsino, S. Giovinazzi, Macroseismic and mechanical models for the vulnerability and damage assessment of current buildings, Bull. Earthq. Eng. 4 (2006) 415–443, https://doi.org/10.1007/s10518-006-9024-z.
[79] C.J. Van Westen, Remote sensing and GIS for natural hazards assessment and disaster risk management, Treatise Geomorphol 3 (15) (2013) 259–298.
[80] A. Roca, X. Goula, T. Susagna, J. Chávez, M. González, E. Reinoso, A simplified method for vulnerability assessment of dwelling buildings and estimation of damage scenarios in Catalonia, Spain, Bull. Earthq. Eng. 4 (2006) 141–158, https://doi.org/10.1007/s10518-006-9003-4.
[81] INE, Instituto Nacional de Estatística, IP - Portugal. [Online]. Available: https://www.ine.pt/xportal/xmain?xpid=INE&xpgid=ine_base_dados (accessed July 2023) .
[82] Google Earth, [Online]. Available: https://www.google.it/earth/(accessed November 2023).
[83] A.N. Martins, C. Forbes, A.A. Pereira, D. Matos, The changing city: risk and built heritage. The case of Lisbon downtown, Procedia Eng. 212 (2018) 921–928, https://doi.org/10.1016/j.proeng.2018.01.119.
[84] Google Earth, [Online]. Available: https://www.google.it/earth/(accessed July 2023).
[85] A.N. Martins, A.A. Pereira, C. Forbes, J.L.M.P. de Lima, D. Matos, Risk to cultural heritage in Baixa Pombalina (Lisbon Downtown)-a transdisciplinary approach to exposure and drivers of vulnerability, Int. J. Architect. Herit. 15 (7) (2021) 1058–1080, https://doi.org/10.1080/15583058.2020.1745322.
[86] J. Nunes, M.J. Neto, Lisbon-between resilience and change: from the 1755 earthquake to the 1988 Chiado fire, in: International Planning History Society Proceedings, TU Delft Open: Carola Hein, Jul. 2016, pp. 391–401, https://doi.org/10.7480/iphs.2016.3.1273.
[87] R. Catulo, A.P. Falcão, R. Bento, S. Ildefonso, Simplified evaluation of seismic vulnerability of Lisbon Heritage City Centre based on a 3DGIS-based methodology, J. Cult. Herit. 32 (2018) 108–116, https://doi.org/10.1016/j.culher.2017.11.014.
[88] L. Dias, F. Braunschweig, N. Grosso, H. Costa, P. Garrett, Flood Risk Mapping. Methodological Guide, 2010.
[89] G. Brando, G. De Matteis, E. Spacone, Predictive model for the seismic vulnerability assessment of small historic centres: application to the inner Abruzzi Region in Italy, Eng. Struct. 153 (2017) 81–96, https://doi.org/10.1016/j.engstruct.2017.10.013.
[90] N. Chieffo, A. Formisano, P.B. Lourenço, Seismic Vulnerability Procedures for Historical Masonry Structural Aggregates: Analysis of the Historical Centre of Castelpoto (South Italy), vol. 48, 2023, pp. 852–866, https://doi.org/10.1016/j.istruc.2023.01.022.
[91] C. Arrighi, M. Brugioni, F. Castelli, S. Franceschini, B. Mazzanti, Flood risk assessment in art cities: the exemplary case of Florence (Italy), Journal of Flood Risk Management 11 (2018) S616–S631, https://doi.org/10.1111/jfr3.12226.
[92] M. Kapović Solomun, C.S.S. Ferreira, V. Zupanc, R. Ristić, A. Drobnjak, Z. Kalantari, Flood legislation and land policy framework of EU and non-EU countries in

Southern Europe, Wiley Interdiscip. Rev. Water 9 (1) (2022) e1566, https://doi.org/10.1002/wat2.1566.
[93] A. Rilo, P. Freire, P.P. Santos, A.O. Tavares, L. Sá, Historical flood events in the Tagus estuary: contribution to risk assessment and management tools, in: Podofillini, et al. (Ed.), Safety and Reliability of Complex Engineered Systems, Taylor and Francis Group, London, 2015, pp. 4281–4286.
[94] M. Leal, C. Ramos, S. Pereira, Different types of flooding lead to different human and material damages: the case of the Lisbon Metropolitan Area, Nat. Hazards 91 (2018) 35–758, https://doi.org/10.1007/s11069-017-3153-3.
[95] M.L.R. Liberato, et al., Moisture sources and large-scale dynamics associated with a flash flood event, in: J. Lin, D. Brunner, C. Gerbig, A. Stohl, A. Luhar, P. Webley (Eds.), Lagrangian Modeling of the Atmosphere, vol. 200, American Geophysical Union, Washington, DC, 2012, pp. 111–126 https://doi.org/10.1029/2012GM001244 [Online]. Available:
[96] M. Fragoso, R.M. Trigo, J.L. Zêzere, M.A. Valente, The exceptional rainfall event in Lisbon on 18 February 2008, Weather 65 (2) (2010) 31–35, https://doi.org/10.1002/wea.513.
[97] IPMA, Instituto Português do Mar e da Atmosfera. [Online]. Available: https://www.ipma.pt/pt/index.html (accessed December 2023) .
[98] APA, Agência Portuguesa do Ambiente. [Online]. Available: https://apambiente.pt/(accessed December 2023) .
[99] S.P. Vilanova, J.F.B.D. Fonseca, Probabilistic seismic-hazard assessment for Portugal, Bull. Seismol. Soc. Am. 97 (5) (2017) 1702–1717, https://doi.org/10.1785/0120050198.
[100] S. Custódio, et al., Earthquakes in western Iberia: improving the understanding of lithospheric deformation in a slowly deforming region, Geophys. J. Int. 203 (1) (2015) 127–145, https://doi.org/10.1093/gji/ggv285.
[101] L. Sá, A. Morales-Esteban, P. Durand Neyra, The 1531 earthquake revisited: loss estimation in a historical perspective, Bull. Earthq. Eng. 16 (2018) 4533–4559, https://doi.org/10.1007/s10518-018-0367-z.
[102] P. Teves-Costa, J. Batllo, J. Cabral, The lower Tagus Valley (Portugal) earthquakes: Lisbon 26 January 1531 and Benavente 23 April 1909, Física Tierra 29 (2017) 61–84 https://doi.org/10.5209/FITE.57599, 2017.
[103] Earthquakelist.org, [Online]. Available: https://earthquakelist.org/(accessed October 2023).
[104] IPQ, NP EN 1998-1:2010, Eurocódigo 8 – Projecto de estruturas para resistência aos sismos. Parte 1: Regras gerais, acções sísmicas e regras para edifícios, 2010.
[105] H. Crowley, et al., European seismic risk model (ESRM20), EFEHR Technical Report 002, V1.0.1 (2021) https://doi.org/10.7414/EUC-EFEHR-TR002-ESRM20 [Online]. Available:
[106] M. Barbato, Y. Li, J. Padgett, Recent advances in assessment and mitigation of multiple hazards, J. Struct. Eng. 143 (9) (2017) 02017001, https://doi.org/10.1061/(ASCE)ST.1943-541X.0001862.
[107] S.S. Yildiz, H. Karaman, Post-earthquake ignition vulnerability assessment of Küçükçekmece District, Nat. Hazards Earth Syst. Sci. 13 (12) (2013) 3357–3368, https://doi.org/10.5194/nhess-13-3357-2013.
[108] L. Milanesi, M. Pilotti, A. Belleri, A. Marini, S. Fuchs, Vulnerability to flash floods: a simplified structural model for masonry buildings, Water Resour. Res. 54 (10) (2018) 7177–7197, https://doi.org/10.1029/2018WR022577.
[109] J. Stolle, et al., Experimental investigation of debris-induced loading in tsunami-like flood events, Geosciences 7 (3) (2017) 74, https://doi.org/10.3390/geosciences7030074.
[110] S. García-Torres, R. Kahhat, S. Santa-Cruz, Methodology to characterize and quantify debris generation in residential buildings after seismic events, Resour. Conserv. Recycl. 117 (2017) 151–159, https://doi.org/10.1016/j.resconrec.2016.11.006.
[111] D. Skoulidou, X. Romão, Are seismic losses affected by the angle of seismic incidence? Bull. Earthq. Eng. 19 (2021) 6271–6302, https://doi.org/10.1007/s10518-021-01121-0.